AGU PUBLICATIONS

JGR

Journal of Geophysical Research: Atmospheres

RESEARCH ARTICLE
10.1002/2017JD026930

Key Points:
- Organic aerosols in Shanghai were characterized, showing that biomass burning and fossil fuel combustion were potentially important sources
- Variations in organic aerosol composition are observed among different months and between daytime and nighttime
- Epoxide-intermediated routes and ammonia-carbonyl chemistry likely dominate the formation of OSs and nitrogen-containing species, respectively

Supporting Information:
- Supporting Information S1
- Data Set S1

Correspondence to:
L. Wang and C. George,
lin_wang@fudan.edu.cn;
christian.george@ircelyon.univ-lyon1.fr

Citation:
Wang, X., Hayeck, N., Brüggemann, M., Yao, L., Chen, H., Zhang, C., … Wang, L. (2017). Chemical characteristics of organic aerosols in shanghai: A study by ultrahigh-performance liquid chromatography coupled with Orbitrap mass spectrometry. *Journal of Geophysical Research: Atmospheres*, *122*, 11,703–11,722. https://doi.org/10.1002/2017JD026930

Received 12 APR 2017
Accepted 10 OCT 2017
Accepted article online 14 OCT 2017
Published online 3 NOV 2017

Chemical Characteristics of Organic Aerosols in Shanghai: A Study by Ultrahigh-Performance Liquid Chromatography Coupled With Orbitrap Mass Spectrometry

Xinke Wang[1], Nathalie Hayeck[2], Martin Brüggemann[2,3], Lei Yao[1], Hangfei Chen[1], Ci Zhang[1], Corinne Emmelin[2], Jianmin Chen[1,4], Christian George[2], and Lin Wang[1,4]

[1]Shanghai Key Laboratory of Atmospheric Particle Pollution and Prevention, Department of Environmental Science and Engineering, Fudan University, Shanghai, China, [2]Université Lyon, Université Claude Bernard Lyon 1 CNRS, IRCELYON, Villeurbanne, France, [3]Now at Leibniz Institute for Tropospheric Research, Leipzig, Germany, [4]Institute of Atmospheric Sciences, Fudan University, Shanghai, China

Abstract Particulate matter 2.5 ($PM_{2.5}$) filter samples were collected in July and October 2014 and January and April 2015 in urban Shanghai and analyzed using ultrahigh-performance liquid chromatography coupled to Orbitrap mass spectrometry. The measured chromatogram-mass spectra were processed by a nontarget screening approach to identify significant signals. In total, 810–1,510 chemical formulas of organic compounds in the negative polarity (negative electrospray ionization (ESI−)) and 860–1,790 in the positive polarity (ESI+), respectively, were determined. The chemical characteristics of organic aerosols (OAs) in Shanghai varied among different months and between daytime and nighttime. In the January samples, organics were generally richer in terms of both number and abundance, whereas those in the July samples were far lower. More CHO− (compounds containing only carbon, hydrogen, and oxygen and detected in ESI−) and CHOS− (sulfur-containing organics) were found in the daytime samples, suggesting a photochemical source, whereas CHONS− (nitrogen- and sulfur-containing organics) were more abundant in the nighttime samples, due to nocturnal nitrate radical chemistry. A significant number of monocyclic and polycyclic aromatic compounds, and nitrogen- and sulfur-containing heterocyclic compounds, were detected in all samples, indicating that biomass burning and fossil fuel combustion made important contributions to the OAs in urban Shanghai. Additionally, precursor-product pair analysis indicates that the epoxide pathway is an important formation route for organosulfates observed in Shanghai. Moreover, a similar analysis suggests that 35–57% of nitrogen-containing compounds detected in ESI+ could be formed through reactions between ammonia and carbonyls. Our study presents a comprehensive overview of OAs in urban Shanghai, which helps to understand their characteristics and sources.

1. Introduction

Organic aerosols (OAs) often represent a main fraction (20%–90%) of submicron atmospheric particulate mass (Jimenez et al., 2009; Kroll & Seinfeld, 2008) and play an important role in determining the climatic and health effects of atmospheric aerosols (Pöschl, 2005). Atmospheric OAs can be divided according to their sources into two categories: primary organic aerosols are directly emitted into the atmosphere from natural or anthropogenic sources, whereas secondary organic aerosols (SOAs) are formed in the atmosphere from precursor gases (Seinfeld & Pankow, 2003). The complexity of OAs dramatically increases through multiple chemical reactions of complex primary organic compounds in the atmosphere (Goldstein & Galbally, 2007) and/or atmospheric aging of OAs (Jimenez et al., 2009; Rudich, Donahue, & Mentel, 2007). Hence, elucidating the chemical composition of the organic fraction in the atmospheric particles at the molecular level is a vital but challenging task.

Traditional methods of OA analysis such as gas chromatography (or liquid chromatography) interfaced with mass spectrometry (GC/MS or LC/MS) can only identify a limited number of highly complex organic compounds in fine aerosol samples, because authentic standards are required to provide retention times in chromatograms and fragmentation patterns in mass spectra. In recent years, methods based on ultrahigh-resolution mass spectrometry (UHRMS, e.g., Fourier transform ion cyclotron resonance mass spectrometry (FTICR-MS) and Orbitrap mass spectrometry) coupled with soft ionization techniques (e.g.,

electrospray ionization, ESI) have been introduced to deliver the exact molecular formulas of the organic components in aerosol particles. The high mass resolution and high mass accuracy of UHRMS allow in many cases the determination of the elemental composition of unknown organic components without the need of authentic standards (Nizkorodov, Laskin, & Laskin, 2011).

Previously, ESI-UHRMS has been used to identify secondary organic compounds generated in laboratory experiments. Reinhardt et al. (2007) identified hundreds of organic compounds generated from α-pinene ozonolysis in a smog chamber using FTICR-MS. Similar techniques were subsequently applied to investigate the chemical composition of SOAs generated from oxidation of isoprene, monoterpenes, diesel fuel, etc., under different conditions (Bateman et al., 2009; Kourtchev et al., 2015; Nguyen et al., 2010, 2011; Romonosky et al., 2017; Walser et al., 2008).

Aerosol samples collected in field campaigns have been analyzed using ESI-HRMS with the objectives to obtain a comprehensive elemental composition of ambient OAs and their plausible sources (Altieri et al., 2012; Kourtchev et al., 2013; Lin et al., 2012; Lin et al., 2012; O'Brien et al., 2013; Rincón et al., 2012; Roach, Laskin, & Laskin, 2010; Tao et al., 2014). For example, Rincón et al. (2012) tentatively identified thousands of organic compounds in the ambient aerosols from Cambridge, UK, and showed that summer samples generally contained more organic components than winter samples. The variation in aerosol composition at the molecular level can be utilized to elucidate the potential sources of ambient aerosols. O'Brien et al. (2014) observed clear diurnal variations of OAs in Bakersfield, CA, USA, and presented evidence of local and long-range transport of SOAs from both biogenic and anthropogenic sources. This technique has been extended to characterize the elemental composition of organic components in aerosols emitted from a specific source (Kourtchev et al., 2016; Laskin, Smith, & Laskin, 2009; Tong et al., 2016). For example, Tong et al. (2016) studied the composition of fine particles at a road tunnel (Queensway) in Birmingham, UK, and concluded that many oxidized particulate monoaromatic, polycyclic aromatic hydrocarbons, and nitrooxy-aromatics originated from vehicle emissions.

Recently, ESI-UHRMS has been combined with LC in a number of studies (Lin et al., 2016; Vogel et al., 2016; Vogel et al., 2016; Wang et al., 2016), which allows separation of isomers and, hence, offers an additional dimension of information in comparison with previous studies using solely direct injection ESI-UHRMS. Another advantage of LC separation is to reduce ion suppression during ionization and to achieve semiquantification of organic compounds. For example, Wang et al. (2016) tentatively identified about 200 formulas of particulate organosulfates (OSs) and dozens of formulas of nitrooxy-OSs, with various numbers of isomers for each determined formula using UHPLC coupled to ESI-Orbitrap MS. It was shown that the abundances of nitrooxy-OSs in the nighttime samples were larger than those in the daytime samples in Shanghai, highlighting the formation of nitrooxy-OSs from the NO_3 nighttime chemistry.

Shanghai is a megacity with extensive emissions of anthropogenic pollutants including particulate matters, volatile organic compounds (VOCs), sulfur dioxide, and nitrogen oxides (Huang et al., 2011; Wang et al., 2013). In previous studies, ESI-UHRMS has been used to determine hundreds of OSs in atmospheric aerosol samples in Shanghai and elucidate their seasonal and diurnal variations (Tao et al., 2014; Wang et al., 2016). Nonetheless, other classes of organic components such as highly oxidized molecules (HOMs) that likely possess extremely low vapor pressure leading to a high mass fraction in the condensed phase (Molteni et al., 2016; Rissanen et al., 2014) remain elusive. In this study, we have determined chemical formulas of compounds containing only carbon, hydrogen, and oxygen (CHO); sulfur-containing organics (CHOS); nitrogen-containing organics (CHON); compounds containing both nitrogen and sulfur (CHONS); and organics without oxygen (CHNS*, including CHN (containing only carbon, hydrogen, and nitrogen), CHS (containing only carbon, hydrogen, and sulfur), and CHNS (containing carbon, hydrogen, nitrogen and sulfur)) in aerosol particles collected in Shanghai, using UHPLC coupled to Orbitrap MS. Data in both polarities were collected: those detected in ESI− were labeled with "−" (e.g., CHO−, CHOS−, CHON−, CHONS−, and CHNS*−), and those detected in ESI+ were labeled with "+" (e.g., CHO+, CHOS+, CHON+, CHONS+, and CHNS*+). In addition, the temporal variations of these species were characterized. Precursor-product pair analysis was utilized to elucidate the formation routes of certain classes of organic compounds. Furthermore, potential sources for OAs in Shanghai will be discussed. Compared with previous studies (Tao et al., 2014; Wang et al., 2016), this study presents a much more comprehensive overview of OAs in urban Shanghai by offering a molecular characterization of extractable particulate organics.

2. Material and Methods

2.1. Sample Collection

Twelve-hour ambient aerosol samples were collected onto 90 mm prebaked quartz-fiber filters (Whatman Company, UK) during 26 to 30 July 2014 (sample ID: July daytime samples, JUD; July nighttime samples, JUN), 19 to 23 October 2014 (sample ID: October daytime samples, OCD; October nighttime samples, OCN), 9 to 11 and 15 to 16 January 2015 (sample ID: January daytime samples, JAD; January nighttime samples, JAN), and 17 to 21 April 2015 (sample ID: April daytime samples, APD; April nighttime samples, APN), using a middle-flow impact aerosol sampler (Qingdao Hengyuan Tech Co., Ltd., HY-100) operating at 100 L min^{-1}. Daytime samples were collected between 8 a.m. and 8 p.m. local time, whereas nighttime samples were collected between 8 p.m. and 8 a.m. the next day. The sampling site was located on the rooftop of a teaching building at Fudan University (31°18′N, 121°30′E), about 20 m above ground with surrounding residential and commercial properties and a major highway to the south of the site (Ma et al., 2014; Xiao et al., 2015). Blank samples were taken following the same procedure except that no air was drawn through the filter substrate. After sample collection, filters were stored at −20°C in a freezer before further analysis. Table S1 in the supporting information provides a comparison of air quality and meteorological conditions during the sampling days in Shanghai.

2.2. Sample Analysis

A quarter of each quartz filter was extracted twice with 6 mL of acetonitrile (Optima® LC/MS, Fischer Scientific, USA) and agitated for 20 min on an orbital shaker set at 1000 rpm. The combined extracts were filtered through a 0.2 μm polytetrafluoroethylene membrane (13 mm, Pall Corporation, USA) using a glass syringe, and then blown to almost dryness under a gentle stream of N_2. The extracts were then reconstituted in 1 mL of a 1:1 vol/vol mixture of water (Optima® LC/MS, Fischer Scientific, USA) and acetonitrile (Optima® LC/MS, Fischer Scientific, USA). For the analysis, 200 μL of the reconstituted extract was diluted by adding 100 μL of water. Five microliter of the diluted solution was analyzed by UHPLC (Dionex 3000, Thermo Scientific, USA) coupled to a Q-Exactive Hybrid Quadrupole-Orbitrap mass spectrometer (Thermo scientific, USA). Three replicate analyses were performed for each extract sample.

In addition, pentafluorobenzylhydroxylamine derivatization was used to identify organic compounds with carbonyl functional groups (Borrás & Tortajada-Genaro, 2012). A volume of 200 μL of the reconstituted extract were mixed with 800 μL of o-(2, 3, 4, 5, 6-pentafluorobenzyl) hydroxylamine hydrochloride (Sigma Aldrich, ≥ 99.0%) solutions (1 mg/mL). The mixture was left in darkness at room temperature for 24 h, then analyzed using the same procedure as previously described.

Analytes were separated using a Waters Acquity HSS T3 column (1.8 μm, 100 × 2.1 mm) with mobile phases consisting of (A) 0.1% formic acid in water (Optima® LC/MS, Fischer Scientific, USA) and (B) 0.1% formic acid in acetonitrile (Optima® LC/MS, Fischer Scientific, USA). Gradient elution was performed by the A/B mixture at a total flow rate of 300 μL/min: 1% B for 2 min, a linear gradient to 100% B in the next 11 min, 100% B for another 2 min, back to 1% B in 0.1 min, and then 1% B for 6.9 min. The Q-Exactive Hybrid Quadrupole-Orbitrap mass spectrometer was equipped with a heated electrospray ionization source, using a spray voltage of −2.6 and 3.2 kV for ESI− and ESI+, respectively. The mass resolving power was 140,000 at *m/z* 200, and the scanning range was set to *m/z* 50–750. The Q-Exactive mass spectrometer was externally mass calibrated daily using a 2 mM sodium acetate solution that provided a series of negative and positive adduct ions in the range of *m/z* 50–750.

2.3. Data Processing

The obtained chromatogram-mass spectra were analyzed by a nontarget approach software (MZmine 2.21), which provides the core functionality for MS data processing: raw data import, peak detection, shoulder peaks filtering, chromatogram building, chromatogram deconvolution, deisotoping, search for adducts and peak complexes, alignment, gap filling, identification, and duplicate peak filtering (Hu et al., 2016; Katajamaa, Miettinen, & Oresic, 2006; Pluskal et al., 2010). The detailed processing steps and settings can be found in the supporting information (Fuller et al., 2012; Hu et al., 2016; Kind & Fiehn, 2007; Lin et al., 2012; Lin et al., 2012; Tao et al., 2014; Wang et al., 2016). The output of MZmine 2.21 includes the *m/z* ratios, formulas, retention times, and abundances of detected organic compounds. Molecular formulas tentatively identified were expressed as $C_cH_hO_oN_nS_s$, where c, h, o, n, and s correspond to the numbers of carbon,

hydrogen, oxygen, nitrogen, and sulfur atoms in the molecular formula, respectively. This molecular formula assignment is mainly based on detected *m/z* values with up to 2 ppm error in the ESI− and 3 ppm error in the ESI+, as well as a number of criteria including the isotope pattern and ratio. Further identity assignments in the following discussion is our best judge based on previous literature reports. Spectra of blank samples were processed using the same settings.

For the chromatogram-mass spectra analysis, the abundance of a compound refers to the average area of its chromatographic peak from the three repetitions and the number of isomers for a compound is based on the number of chromatographic peaks observed for a given *m/z* value. The obtained number of isomers may vary significantly when the separation method is further optimized (Wang et al., 2016). Also, the spiky or irregular shapes of some peaks may lead to uncertainties in the number of isomers. The compound list for the blank samples was compared to those for ambient samples, and only compounds with a sample-to-blank abundance ratio ≥10 were retained. Subsequently, the abundance of the retained compounds in the ambient samples was blank-corrected. Then, the arbitrary abundances of all isomers for a given formula were added up. The intensity variability due to instrumental performance was taken into account through daily analysis of standards. The relative standard deviations of imidazole carboxaldehyde, adicpic acid, sodium methyl sulfate, camphor sulfonic acid, sodium octyl sulfate, and sodium dodecyl sulfate in the standard solutions that were analyzed daily were lower than 11%.

Ring and double-bond equivalence (RDBE) provides information on the number of rings and double bonds in the molecules. RDBE is usually calculated as

$$\mathrm{RDBE} = \frac{2c + 2 + n - h}{2} \tag{1}$$

However, it should be noted that RDBE for compounds with heteroatoms (e.g., O, N, and S) may not accurately indicate the level of unsaturation. For example, the two S═O double bonds in sulfate groups are not taken into account when calculating the unsaturation degree of OSs based on equation (1) (Wang et al., 2016).

The aromaticity equivalent (Xc) has been suggested to improve identification and characterization of monocyclic and polycyclic aromatic compounds (Tong et al., 2016; Yassine et al., 2014). Xc for compounds containing only carbon, hydrogen, nitrogen, oxygen, sulfur, and phosphorus can be calculated as follows:

$$\mathrm{Xc} = \frac{3(\mathrm{RDBE} - (p \times o + q \times s)) - 2}{\mathrm{RDBE} - (p \times o + q \times s)} \tag{2}$$

where p and q, respectively, correspond to the fraction of oxygen and sulfur atoms involved in π-bond structures of a compound that varies depending on the category of the compound. For example, carboxylic acids, esters, and nitro compounds are characterized by p = q = 0.5. For compounds containing carbonyl, nitroso, cyano, hydroxyl, or ether functionalities, p and q could be either 1 or 0. In this study, p = q = 0.5 was used for compounds detected in ESI−, because ESI− is more sensitive to compounds containing carboxylic groups (Kourtchev et al., 2016; Tong et al., 2016). However, p = q = 1 was selected in ESI+, because compounds with a large diversity of functional groups can possibly be detected. The selection of these values for p and q is attempting to avoid an overestimation of the amount of monocyclic and polycyclic aromatics; however, it could have led to underestimations (Yassine et al., 2014). For molecular formulas with an odd number of oxygen or sulfur, the sum (p × o + q × s) in equation (2) was rounded to the next lower integer (Yassine et al., 2014). Xc ≥ 2.50 and Xc ≥ 2.71, respectively, are proposed as unambiguous minimum criteria for the presence of mono- and polycyclic aromatics.

Carbon oxidation state (OS_C) was introduced as a preferred metric for the degree of oxidation of organic species in the atmosphere, compared to the simple but more error-prone use of O/C ratios. For organic compounds composed of carbon, hydrogen, and reduced oxygen, OS_C can be calculated through the following equation (Kroll et al., 2011):

$$\mathrm{OSc} \approx 2\mathrm{O/C} - \mathrm{H/C} \tag{3}$$

where O/C and H/C are the elemental ratio of oxygen-to-carbon and hydrogen-to-carbon, respectively. The presence of peroxide groups (in which the oxygen atoms have an oxidation state of −1) and heteroatoms (which can have a range of oxidation states) introduces deviations from this relation (Kroll et al., 2011).

The Kendrick mass defect (KMD) is very useful to differentiate a group of similar compounds among a large set of molecular formulas obtained by UHRMS (Hughey et al., 2001; Kendrick, 1963). In this study, CH_2 (14.00000) was chosen as a base unit, and equations (4) and (5) were used to calculate the Kendrick mass (KM_{CH2}) and the Kendrick mass defect (KMD_{CH2}), respectively:

$$KM_{CH_2} = \text{Observed Mass} \times \left(\frac{14.00000}{14.01565}\right) \tag{4}$$

$$KMD_{CH_2} = \text{Nominal Mass} - KM_{CH_2} \tag{5}$$

where "Observed Mass" is the exact mass of a compound calculated from the *m/z* value measured by the mass spectrometer and "Nominal Mass" is the rounded integer mass of a compound (Wang et al., 2016).

3. Results and Discussion

3.1. General Characteristics

A main emphasis of this study is to tentatively identify the broad and complex composition of organic compounds in ambient aerosol samples from Shanghai and compare the characteristics among different months and between daytime and nighttime. Hence, the list of molecular formulas from each sample was compared with that from the blank sample as discussed above, and then intercompared with those from samples collected in the same month. Only compounds observed in all daytime or all nighttime samples for a particular month were considered as representative species and included for further discussion. As discussed in the previous session, LC separation helps reduce ion suppression effects and achieve semiquantification of organic compounds. In the following, we focus on a statistical and comprehensive picture of the formulas and abundances of organic species in Shanghai aerosol samples, and the number of isomers is not regarded as a key output at this point.

The assigned formulas can be subdivided into five groups: compounds containing only carbon, hydrogen, and oxygen (CHO); sulfur-containing organics (CHOS); nitrogen-containing organics (CHON); compounds containing both nitrogen and sulfur (CHONS); and organics without oxygen (CHNS*, including CHN, CHS, and CHNS). The number of molecular formulas tentatively identified in each month including the number for each subgroup is listed in Tables S2–S5. Overall, 810–1,510 and 860–1,790 molecular formulas of organic compounds with various numbers of isomers for each formula were determined in ESI− and ESI+, respectively. The greatest number of formulas was detected in the January samples in both ESI− and ESI+, whereas the number of formulas in the July samples was far lower compared to those in the other three months, showing an opposite trend to previous measurements in Cambridge, UK (Rincón et al., 2012). This contrasting observation can be explained by the backward trajectories from the sampling site depicted in Figure S1 in the supporting information. These trajectories show that during winter the air masses originated from northern China with extensive emissions of anthropogenic pollutants from fossil fuel combustion and biomass burning (Huang et al., 2014; Zha et al., 2014) resulting in the highest concentrations of particulate matter 2.5 ($PM_{2.5}$) and correspondingly a high number of organic compounds, whereas most of air masses came from the clean ocean with the lowest concentrations of $PM_{2.5}$ and particulate organics during the July sampling period (Figure S1 and Table S1). In addition, the boundary layer is normally higher in summer and lower in winter, leading to a higher abundance of organics in January in Shanghai. Nonetheless, it should be noted that the number of formulas did not show a prominent diurnal difference (Tables S2–S5).

Mass spectra of urban atmospheric OAs were reconstructed in both ESI− (Figure 1) and ESI+ (Figure 2). It should be noted that liquid chromatography in front of the mass spectrometer could greatly resolve ion suppression effect, but uncertainties exist when comparing the abundances of organics in different categories because of their different detection sensitivity. In this study, all species are assumed to have the same

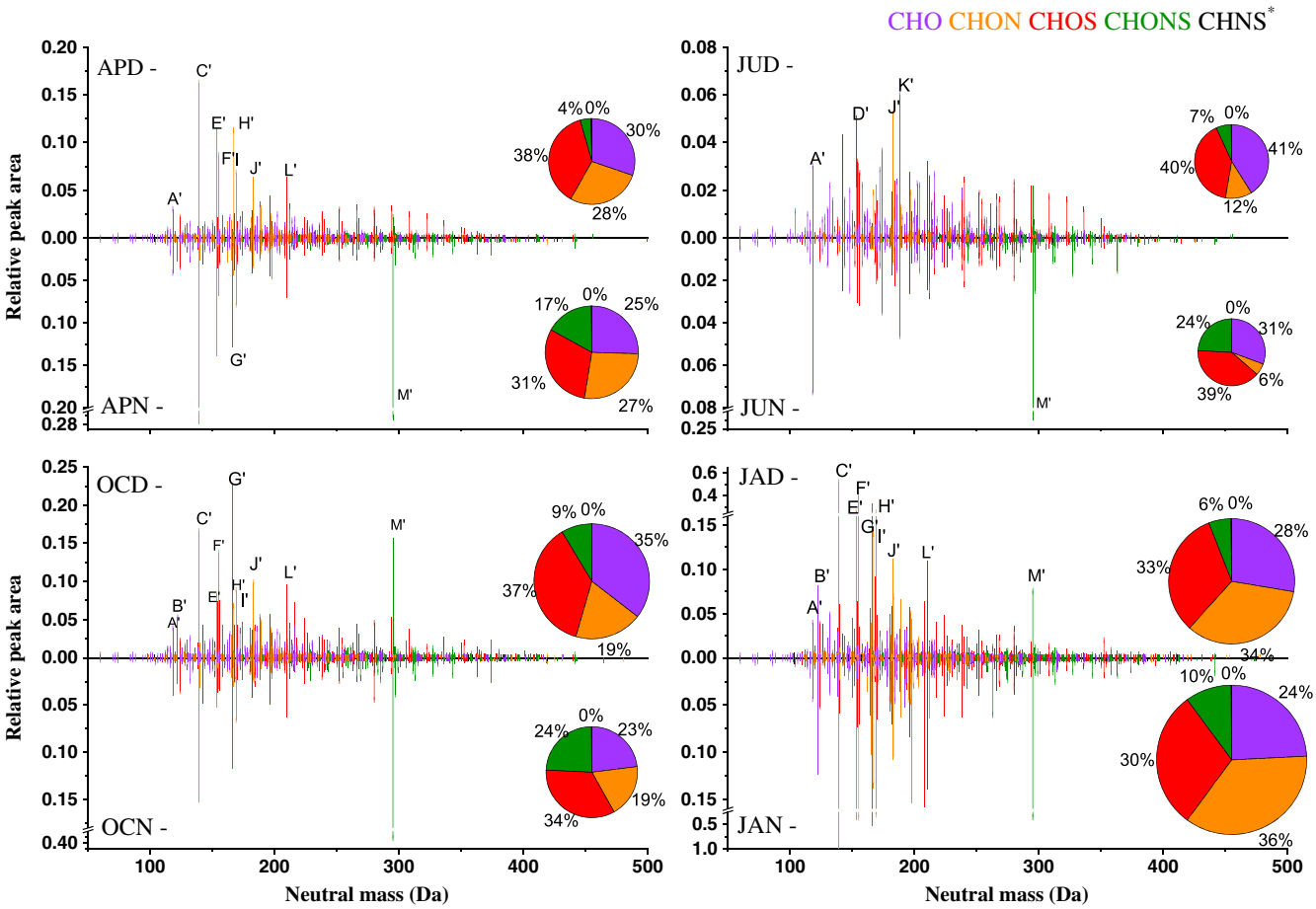

Figure 1. Mass spectra of detected CHO−, CHOS−, CHON−, CHONS−, and CHNS*− reconstructed from extracted ion chromatograms (UHPLC-Orbitrap MS analysis, ESI−). Note that the average abundance of $C_6H_5NO_3$ in the January nighttime samples (the highest one from all samples) was set arbitrarily to 100%. The sizes of pie charts are proportional to the added-up abundances of all species for a subgroup in the five samples of a particular month. APD, April daytime samples; APN, April nighttime samples; JUD, July daytime samples; JUN, July nighttime samples; OCD, October daytime samples; OCN, October nighttime samples; JAD, January daytime samples; JAN, January nighttime samples.

signal response and the total peak areas of organics are compared among different samples. In both ESI− and ESI+, the January samples showed the highest total abundance of detected compounds, whereas the total abundance in the July samples was far lower than those in the other three months, similar to the trend in the number of organic compounds tentatively identified (Tables S2–S5). In Figure 1, CHO− accounted for a significant percentage in terms of abundance in each month and its fraction was the highest in the July samples. Thus, daytime samples were generally richer in CHO− than nighttime samples, indicating a photochemical formation route of CHO− compounds. The abundance of CHOS− showed the same trend with that of CHO−, also suggesting a photochemical formation route of these multifunctional compounds (Nozière et al., 2010; Rincón et al., 2012; Schindelka et al., 2013). In contrast, the abundances of CHONS− were far higher in nighttime samples than those in daytime samples, probably due to nighttime NO_3 chemistry (Hatch et al., 2011; Wang et al., 2016). The abundance of CHON− showed no obvious diurnal variations, suggesting diverse sources.

For each of the organic compounds with the strongest arbitrary abundance in Figure 1, the formula, RDBE, Xc, and potential source/precursor are listed in Table 1. Most of these compounds were probably aromatics ($Xc \geq 2.50$, such as $C_6H_5NO_3$ (nitrophenol)) with a high degree of unsaturation. Their potential sources include biomass burning and vehicular emissions, important sources for organic compounds in urban atmosphere (Iinuma et al., 2010; Lin et al., 2012; Mohr et al., 2013; Simoneit et al., 2003; Vogel et al., 2016). On the other hand, K′ ($C_8H_{12}O_5$) and M′ ($C_{10}H_{17}NO_7S$) were probably oxidation products of monoterpenes

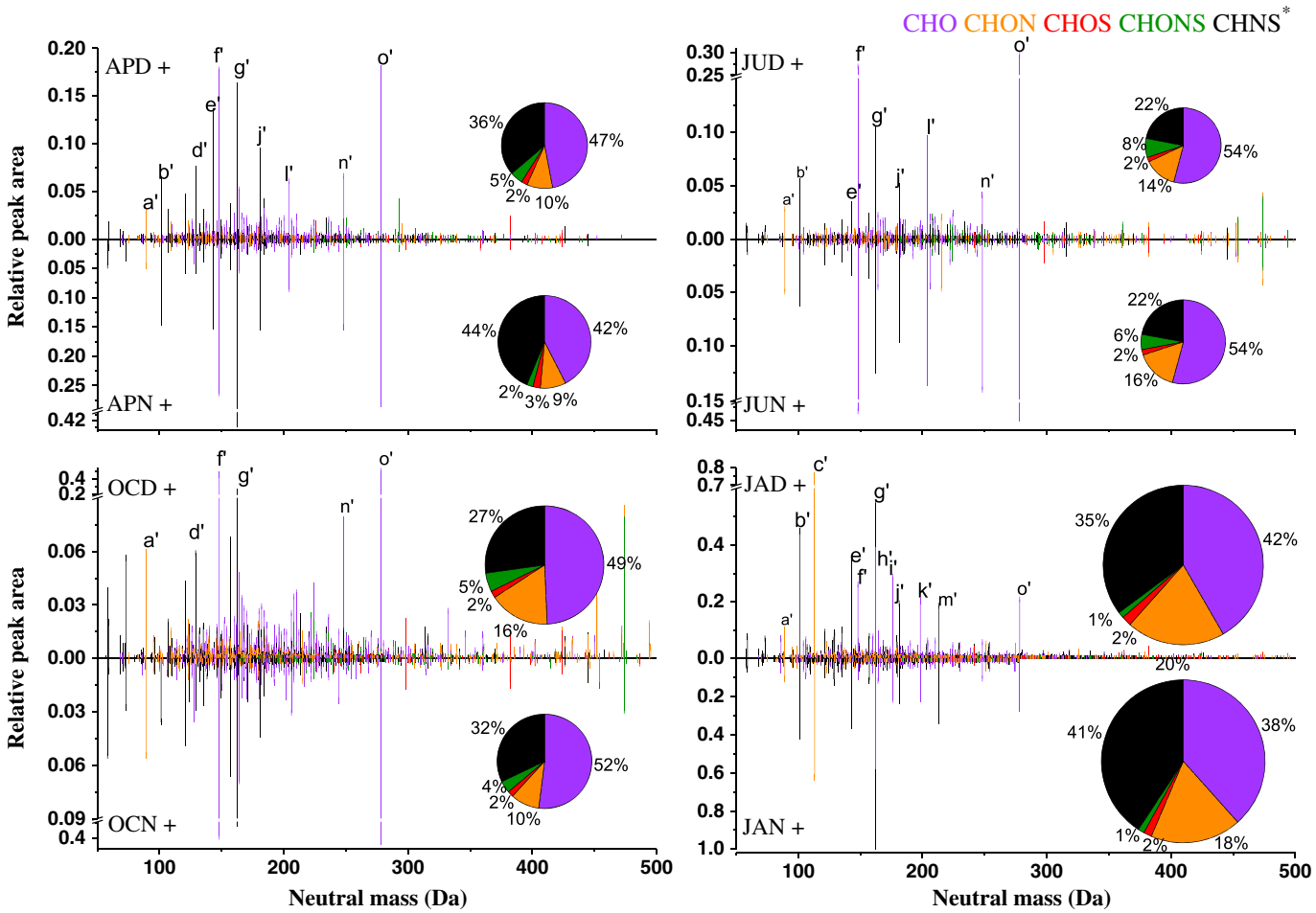

Figure 2. Mass spectra of detected CHO+, CHOS+, CHON+, CHONS+, and CHNS*+ reconstructed from extracted ion chromatograms (UHPLC-Orbitrap MS analysis, ESI+). Note that the average abundance of $C_{10}H_{14}N_2$ in the January nighttime samples (the highest one from all samples) was set arbitrarily to 100%. The sizes of pie charts are proportional to the added-up abundances of all species for a subgroup in the five samples of a particular month. APD, April daytime samples; APN, April nighttime samples; JUD, July daytime samples; JUN, July nighttime samples; OCD, October daytime samples; OCN, October nighttime samples; JAD, January daytime samples; JAN, January nighttime samples.

(Gómez-González et al., 2012; Riva et al., 2015; Surratt et al., 2008), suggesting that biogenic sources could have made a contribution to the loading of OAs.

A major difference between the mass spectra measured in ESI− and ESI+ is the higher percentage of CHN and CHNS compounds in ESI+, in terms of both number and abundance (Tables S2–S5 and Figures 1 and 2). This is mainly due to the fact that amines are more easily detected in ESI+ (Rincón et al., 2012). In Figure 2, the peak area of CHO+ and CHNS*+ accounted for 76–90% of the total abundance, far greater than the others. The total peak area of CHON+ was less than 20% and their number accounted for more than 31% (Tables S2–S5). Both the number and abundance of CHOS+ and CHONS+ represented a few percent of the total abundance.

For each of the ESI+ compounds with the strongest abundance, the formula, RDBE, Xc, and potential source/precursor are also listed in Table 1. Most of these compounds contained reduced nitrogen based on their O/N ratios, indicating amines or amides from direct emissions of industry and tobacco smoke (Ge, Wexler, & Clegg, 2011; Schmeltz & Hoffmann, 1977). In addition, a number of aliphatic alcohols and carbonyls with long carbon chains showed high abundances, probably from the vehicle emissions (Jakober et al., 2006; Williams et al., 2012).

The difference between daytime and nighttime samples was less prominent in terms of assigned formulas. About 69–85% of the compounds detected in ESI− were present in both daytime and nighttime samples.

Table 1
Potential Identities and Sources for the Most Intense Species From ESI− (Figure 1) and ESI+ (Figure 2) Mass Spectra

ID[a]	Neutral mass	Formula	RDBE[b]	Xc	Potential identity	Potential source/precursor	Reference
A′	118.0264	$C_4H_6O_4$	2	0.00	Succinic acid	-	(Xu & Zhang, 2012)
B′	122.0366	$C_7H_6O_2$	5	2.50	Benzoic acid	Naphthalene	(Riva et al., 2015)
C′	139.0268	$C_6H_5NO_3$	5	2.50	Nitrophenol	Biomass burning	(Mohr et al., 2013)
D′	153.0094	$C_3H_7NO_4S$	1	0.00	-	-	-
E′	153.0424	$C_7H_7NO_3$	5	2.50	Methylnitrophenol	Biomass burning	(Mohr et al., 2013)
F′	155.0217	$C_6H_5NO_4$	5	2.33	Nitrocatechols	Biomass burning and vehicle emissions	(Kourtchev et al., 2016) and references therein
G′	166.0264	$C_8H_6O_4$	6	2.50	Phthalic acid	Naphthalene	(Riva et al., 2015)
H′	167.0580	$C_8H_9NO_3$	5	2.50	Benzene compound	-	(Lin et al., 2012)
I′	169.0473	$C_7H_7NO_4$	5	2.33	Methyl-nitrocatechols	Biomass burning and diesel exhaust	(Iinuma et al., 2010)
J′	183.0166	$C_7H_5NO_5$	6	2.50	3-/ 5-Nitrosalicylic acid	Biomass burning	(Kitanovski et al., 2012)
K′	188.0681	$C_8H_{12}O_5$	3	1.00	Unknown terpenoic acid	α-pinene; β-pinene	(Gómez-González et al., 2012)
L′	210.0921	$C_8H_{18}O_4S$	0	0.00	Aliphatic organosulfate	Biodiesel and diesel fuel	(Blair et al., 2017)
M′	295.0721	$C_{10}H_{17}NO_7S$	3	0.00	Pinanediol mononitrate	α-pinene; β-pinene; α-terpinene; Terpinolene	(Gómez-González et al., 2012)
a′	89.0838	$C_4H_{11}NO$	0	0.00	Dimethylethanolamine; Isobutanolamine	CO_2 capture; Industry	(Ge et al., 2011) and references therein
b′	101.1201	$C_6H_{15}N$	0	0.00	Triethylamine; Hexylamine; Dipropylamine; Diisopropylamine; n-Propylisopropylamine	Cattle; swine; solvent; sewage; ambient air; Tobacco smoke	(Ge et al., 2011) and references therein
c′	113.0838	$C_6H_{11}NO$[c]	2	1.00	ε-Caprolactam	Industry	(Cheng, Li, & Leithead, 2006)
d′	129.0577	C_9H_7N	7	2.71	Quinoline	Tobacco smoke	(Schmeltz & Hoffmann, 1977)
e′	143.0733	$C_{10}H_9N$	7	2.71	1-Naphthalenamine; 2-Naphthylamine	Aluminum smelter; tobacco smoke	(Ge et al., 2011) and references therein
f′	148.0159	$C_8H_4O_3$	7	2.50	Phthalic anhydride	Naphthalene	(Riva et al., 2015)
g′	162.1154	$C_{10}H_{14}N_2$	5	2.60	Nicotine	Tobacco smoke	(Schmeltz & Hoffmann, 1977)
h′	162.1251	$C_8H_{18}O_3$	0	0.00	Aliphatic alcohol	-	(Yao et al., 2016)
i′	176.1044	$C_8H_{16}O_4$[c]	1	0.00	Aliphatic carbonyl	-	(Lin et al., 2012)
j′	181.1826	$C_{12}H_{23}N$	2	2.00	Dodecanenitrile	Biomass burning	(Simoneit et al., 2003)
k′	198.1614	$C_{12}H_{22}O_2$[c]	2	0.00	Aliphatic carbonyl	-	(Lin et al., 2012)
l′	204.0783	$C_{12}H_{12}O_3$[c]	7	2.50	Benzene compound	-	(Lin et al., 2012)
m′	213.2451	$C_{14}H_{31}N$	0	0.00	C_{14} Amine	-	(Roach et al., 2010)
n′	248.1981	$C_{13}H_{28}O_4$	0	0.00	Aliphatic alcohol	-	-
o′	278.1512	$C_{16}H_{22}O_4$	6	2.00	Aliphatic acid	-	(Lin et al., 2012)

[a]Peak IDs correspond to the peak labels in Figures 1 and 2. [b]Ring and double bond equivalence (RDBE) are calculated based on equation (1). [c]A molecule contains at least one carbonyl functional group.

Similarly, about 66–79% of the compounds in ESI+ were found to be identical between daytime and nighttime samples. Therefore, in the following discussion, formulas and their abundances of daytime and nighttime samples were combined for simplicity, just as if a 24 h sample were collected instead of a 12 h daytime sample and a 12 h nighttime sample. On the other hand, only 10–13% of compounds were detected in both polarities, suggesting a general significant difference between compounds detected by ESI− and ESI+. This is due to the differences between negative and positive ionization mode mechanisms in the electrospray (i.e., mainly due to the acidity of the analytes). ESI− is especially sensitive to deprotonatable compounds such as organic acids, whereas basic compounds are commonly protonated in the electrospray and, thus, detected in ESI+ (Cech & Enke, 2001; Lin et al., 2012).

3.2. CHO Compounds

In total, 333–502 formulas of CHO− and 365–603 formulas of CHO+ compounds were determined. In Figures 1 and 2, these CHO− and CHO+ compounds, shown in purple, covered wide ranges of molecular weights from 60 to 400 Da and 70 to 500 Da, respectively. The mass spectra peaks with the highest abundances were centered around 120–250 Da and 140–280 Da, respectively.

Figure 3 presents the OS_C versus carbon number plots for the CHO− compounds for each month. The detected CHO− compounds exhibited up to 24 carbon atoms and covered a wide mass range from 50 to

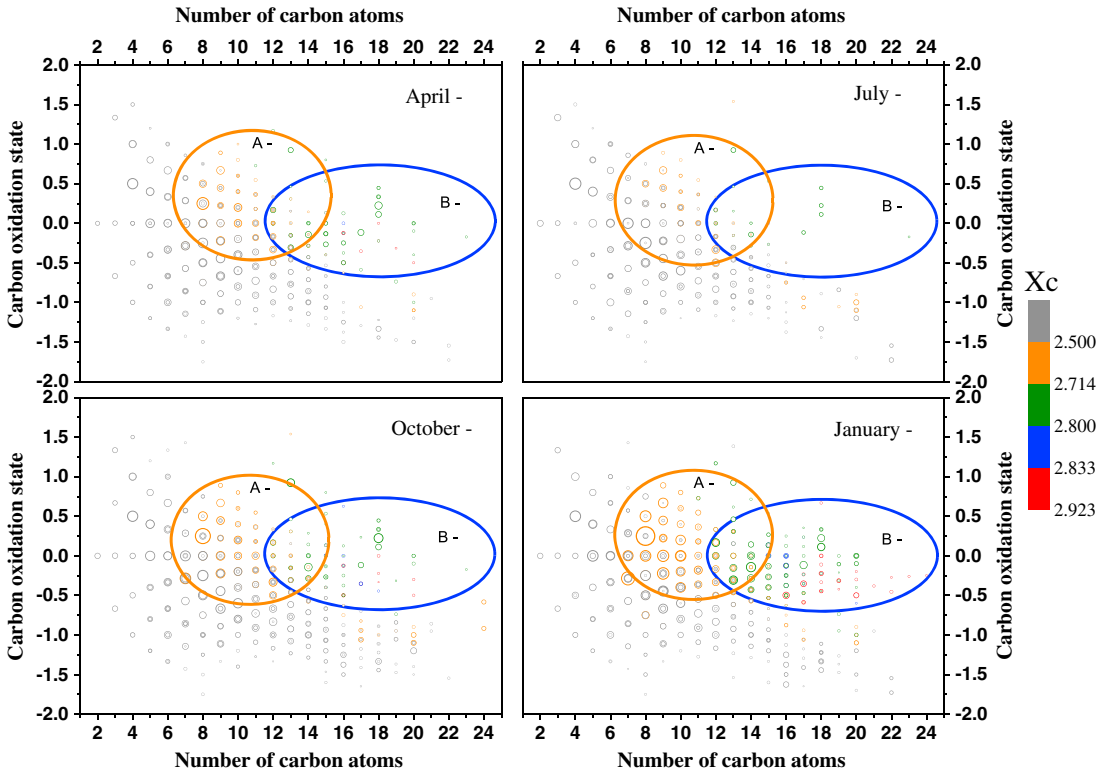

Figure 3. Carbon oxidation state (OS_C) plots for CHO− compounds. The color-coding indicates the Xc values calculated from equation (2). The grey, orange, green, blue, and red circles represent aliphatic compounds (Xc < 2.50), aromatics with a benzene core structure (2.50 ≤ Xc < 2.71), with a naphthalene (2.71 ≤ Xc < 2.80) core structure, with an anthracene (2.80 ≤ Xc < 2.83) core structure, and with a pyrene core structure (2.83 ≤ Xc < 2.92), respectively. The size of symbols is proportional to the fourth root of the abundance of a compound. The ovals (i.e., regions A− and B−) represent where the majority of monocyclic and polycyclic aromatics, respectively, are expected to occur.

400 Da (Figure 1), showing OS_C from −1.8 to +1.5 in the four months (Figure 3). In agreement, Tong et al. (2016) obtained the similar trend of OS_C versus carbon number in a previous study on the molecular composition of OAs at road tunnel sites. Many earlier studies suggest that a molecule with an OS_C between −1 and +1 and with less than 14 carbon atoms can be attributed to semivolatile and/or low-volatility oxidized organic aerosol components (SV-OOA and LV-OOA), which are produced by multistep oxidation reactions. In contrast, molecules with an OS_C between −0.5 and −1.5 and with more than six carbon atoms should be regarded as primary biomass burning organic aerosol (BBOA), which is directly emitted into the atmosphere (Kourtchev et al., 2015; Kourtchev et al., 2016; Kroll et al., 2011). In this study, most of the CHO− compounds were in the region of SV-OOA and LV-OOA, accounting for 56%, 67%, 71%, and 57% of the total CHO− compounds in January, April, July, and October samples, respectively. It seems clear that the majority of monoaromatics gave signals in region (A−) (Figure 3) where the OS_C lies between −0.5 and 1.0 and the carbon number is between 7 and 15. Consistent with the lower OS_C and longer carbon numbers of polycyclic aromatics, the majority of these signals were found in region (B−) where the OS_C is between −0.75 and 0.5 and the carbon numbers are between 12 and 24. In addition, an obvious variation in the number and abundance of monocyclic and polycyclic aromatics was observed among different months. For the January samples, the number of monocyclic and polycyclic aromatics accounted for 24% and 27% of total CHO− compounds, respectively, greater than those in the other three months. The number of monocyclic and polycyclic aromatics in the July samples was the lowest, being only 22% and 7% of total CHO− compounds, respectively. These results suggested that anthropogenic source made the most important contributions to the OAs of Shanghai in winter.

Not surprisingly, CHO+ compounds came with lower OS_C (from −1.75 to 0.5) compared with CHO− compounds (Figure 4). In addition, most of the CHO+ compounds were in the region of BBOA, making up

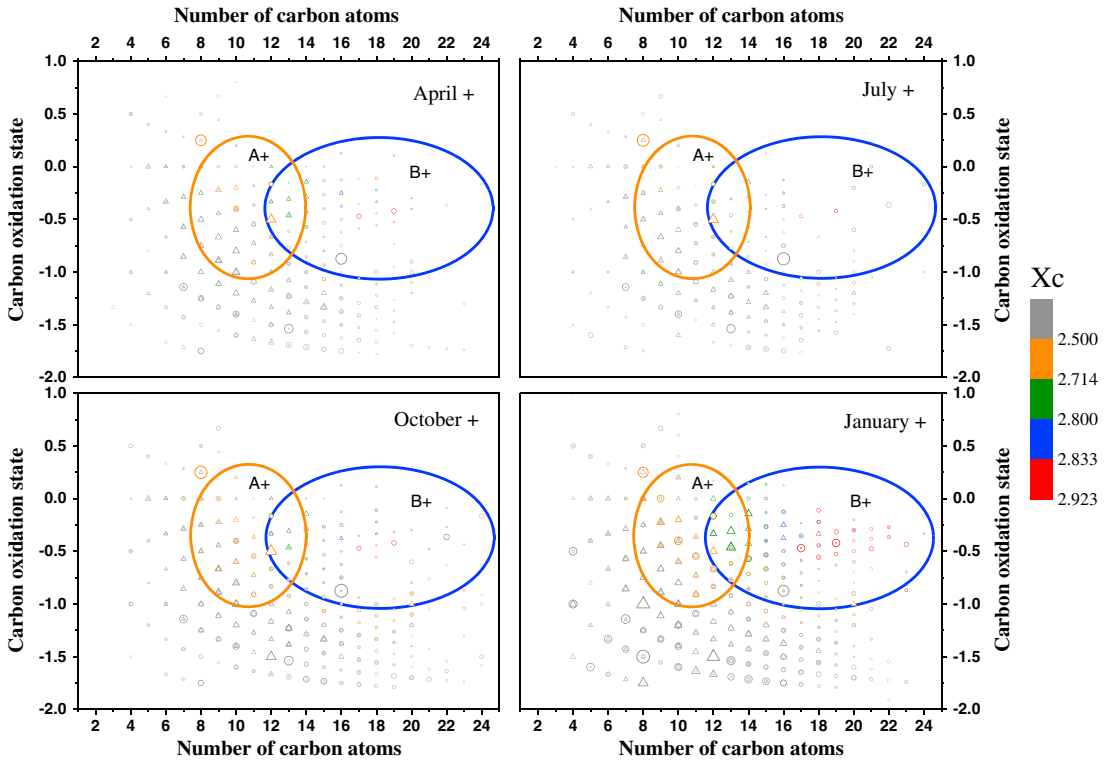

Figure 4. Carbon oxidation state (OS_C) plots for CHO+. The color-coding indicates the Xc values calculated from equation (2), and triangles denote compounds containing at least one carbonyl functional group. The grey, orange, green, blue, and red circles represent aliphatic compounds (Xc $<$ 2.50), aromatics with a benzene core structure (2.50 $\leq$ Xc $<$ 2.71), with a naphthalene (2.71 $\leq$ Xc $<$ 2.80) core structure, with an anthracene (2.80 $\leq$ Xc $<$ 2.83) core structure, and with a pyrene core structure (2.83 $\leq$ Xc $<$ 2.92), respectively. The size of symbols is proportional to the fourth root of the abundance of a compound. The ovals (i.e., regions A + and B+) represent where the majority of monocyclic and polycyclic aromatics, respectively, are expected to occur.

to 56%, 55%, 63%, and 60% of the total CHO+ compounds in January, April, July, and October samples, respectively. These high percentages suggest that primary organic compounds directly emitted from biomass burning were preferably detected in ESI+. A large number of monocyclic and polycyclic aromatics were located in the regions (A+) and (B+) in Figure 4, showing the same trend in number as those detected in ESI−, that is, the highest for the January samples (20% for the monoaromatics and 18% for the polycyclic aromatics) and the lowest for the July samples (18% for the monoaromatics and 7% for the polycyclic aromatics). However, while regions (A+) and (B+) had similar ranges of carbon numbers compared to (A−) and (B−), lower ranges of OS_C were observed (−1.0–0.25 for both region (A+) and region (B+)), indicating that the monocyclic and polycyclic aromatics detected in ESI+ were more reduced than those detected in ESI−.

The triangles in Figure 4 denote the presence of carbonyl functional group(s) in the compound based on pentafluorobenzylhydroxylamine derivatization. A total of 132–183 CHO+ compounds contain at least one carbonyl functional group, accounting for 30–40% of the total in Shanghai. The majority of formulas containing carbonyl functional group(s) are present in the molecular weight range from 70 to 300 Da. However, it should be noted that carbonyl groups in a compound with a neutral mass greater than 554 Da could not be differentiated using pentafluorobenzylhydroxylamine derivatization, since the scanning range of MS was limited to *m/z* 50–750.

Van Krevelen (VK) diagrams can be used to describe the overall compositional characteristics of complex organic mixtures. The most oxidized species lie at the lower right, whereas the most reduced/saturated species lie at the upper left of the VK diagram where the H/C ratio of each compound in the mass spectrum is plotted versus its O/C ratio (Kim, Kramer, & Hatcher, 2003; Wu, Rodgers, & Marshall, 2004), as shown in Figures 5 and S2. In Figures 5 and S2 and Tables S2–S5, O/C values for CHO− compounds were obviously

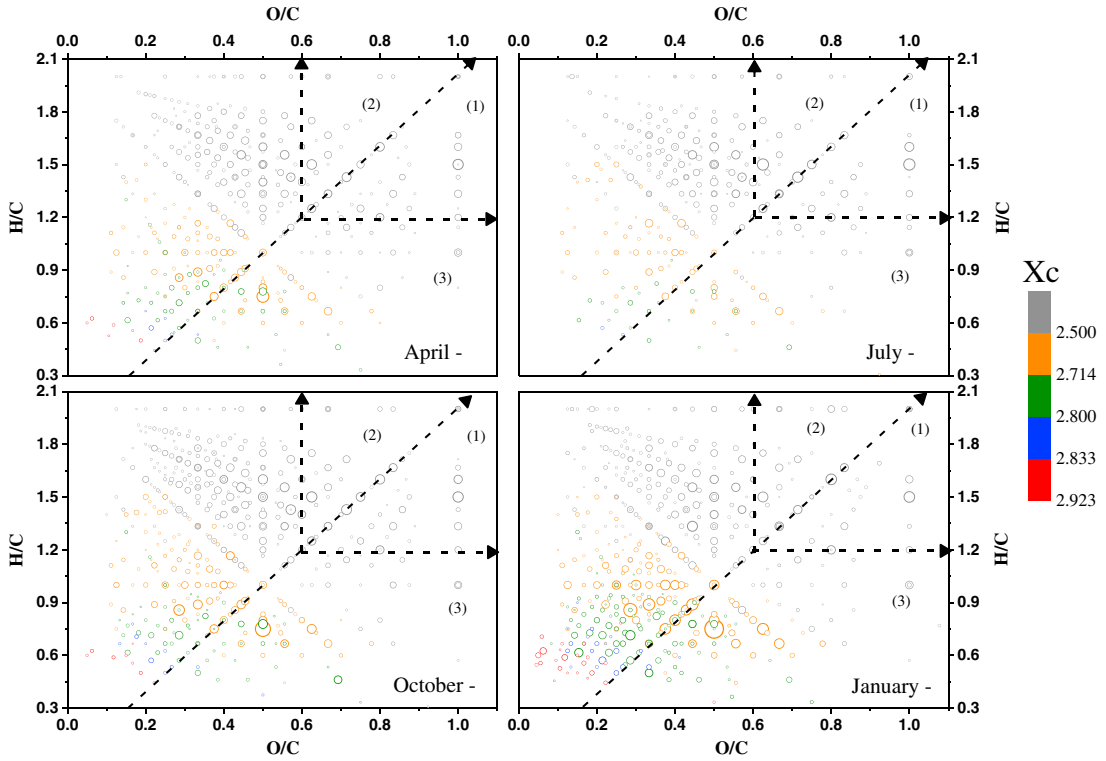

Figure 5. Van Krevelen (VK) diagrams of CHO− compounds. The color-coding indicates the Xc values calculated from equation (2). The grey, orange, green, blue, and red circles represent aliphatic compounds (Xc < 2.50), aromatics with a benzene core structure (2.50 ≤ Xc < 2.71), with a naphthalene (2.71 ≤ Xc < 2.80) core structure, with an anthracene (2.80 ≤ Xc < 2.83) core structure, and with a pyrene core structure (2.83 ≤ Xc < 2.92), respectively. The size of symbols is proportional to the fourth root of the abundance of a compound.

greater than those of CHO+ compounds, likely due to the more favorable ionization of carboxylic acids in the negative polarity.

HOMs that could play an important role in the new particle formation (Bianchi et al., 2016) and contribute to the loading of OAs (Molteni et al., 2016; Rissanen et al., 2014) are clearly visualized in the VK diagrams. Defined as formulas with O/C ≥ 0.6 and/or $OS_C \geq 0$, HOMs can be subdivided into three groups: those containing a great fraction of oxidized functional groups (acids and carbonyls) in region (1) (O/C ≥ 0.6 and $OS_C \geq 0$), those containing a great fraction of reduced functional groups (for instance, alcohols, esters, and peroxides) in region (2) (O/C ≥ 0.6 and $OS_C < 0$), and those with a moderate level of oxygenation in region (3) ($OS_C \geq 0$ and H/C ≤ 1.2) (Tu, Hall, & Johnston, 2016). The number and percentage of HOMs in region (1), region (2), and region (3) for each month are tabulated in Table S6. HOMs accounted for 33–40% of the CHO− compounds in ESI−, and 8–12% in ESI+. More than 50% of HOMs were located in region (3) for both polarities, indicating that most HOMs in urban Shanghai were at a moderate level of oxygenation. Recently, Molteni et al. (2016) identified more than 100 HOMs derived from OH radical-initiated reactions of anthropogenic volatile organic compounds (AVOCs, such as benzene, toluene, xylenes, and trimethylbenzenes). Between 31 and 44 of them were present in our samples (in ESI−), accounting for 18–29% of total numbers and 11–31% of total abundances of HOMs−. The highest abundance in the July samples and the lowest in the January samples suggest that photooxidation of AVOCs is probably an important source for HOMs in Shanghai.

3.3. CHON Compounds

CHON compounds represented a significant percentage of organic compounds in terms of both number and abundance (Figures 1 and 2 and Tables S2–S5). Overall, 168–373 CHON− compounds were observed, compared to 308–698 CHON+ compounds. In general, the CHON compounds covered wide mass ranges with averages around 225 Da in ESI− and 240 Da in ESI+, respectively (Figures 1 and 2).

As can be seen from Figure S3, O/C values for the majority of CHON− compounds were in the range of 0–1.2, and the average O/C values in each month were around 0.5. Since the ranges of O/C values are too broad to be compared between different regions, we focus our attention on the average O/C ratios: slightly lower values were previously reported for measurements in the Pearl River Delta region, but higher values were found in Cambridge, UK, and Bakersfield, CA, USA (Kourtchev et al., 2016; Lin et al., 2012; O'Brien et al., 2014; Rincón et al., 2012). In addition, only around 50% of CHON− compounds were characterized by $O/N \geq 3$, which is far lower than that in Bakersfield, CA, USA, and possibly indicating more reduced nitrogen-containing compounds in Shanghai. In all four months, aromatics accounted for more than 65% of the CHON− compounds, of which 23–27% accounted for polycyclic aromatics. The majority of aromatics were in the region between $0.3 < H/C < 2$ and $0 < O/C < 0.9$, showing their low degrees of oxidation and saturation. Nitrooxy-aromatic compounds such as nitrophenols ($C_6H_5NO_3$), methylnitrophenol ($C_7H_7NO_3$), nitrocatechol ($C_6H_5NO_4$), and methyl-nitrocatechols ($C_7H_7NO_4$) were always abundant in Shanghai (Figure 1 and Table 1) and were in the past often attributed to OAs from biomass burning (Iinuma et al., 2010; Kitanovski et al., 2012; Kitanovski et al., 2012; Kourtchev et al., 2016; Mohr et al., 2013). Furthermore, these compounds were proposed to be potential contributors to light absorption in organic aerosol particles (Laskin, Laskin, & Nizkorodov, 2015). It should be noted that Xc values for $C_6H_5NO_4$ and $C_7H_7NO_4$ are lower than 2.50, suggesting that the amount of aromatics could have been underestimated. In addition, the polycyclic aromatics were characterized by lower H/C and O/C ratios, such as nitronapthol ($C_{10}H_7NO_3$) and methylnitronapthol ($C_{11}H_9NO_3$) in the triangle region of $0.3 < H/C < 1.2$ and $0 < O/C < 0.6$.

In Figure S4, the majority of the CHON+ compounds are located in the range of $0.3 < H/C < 3$ and $0 < O/C < 0.6$, consistent with previous studies (O'Brien et al., 2013; Rincón et al., 2012), indicating that they were more reduced and saturated than CHON− compounds. The 28–110 CHON formulas with more than one oxygen atom were detected in both ESI− and ESI+ in the four-month samples. Thus, these are compounds that contain both acidic (−COOH) and basic($-NH_2$) functional groups, which may include amino acids (Lin et al., 2012) that were previously identified as an important class of dissolved organic nitrogen in aerosol particles (Zhang, Anastasio, & Jimemez-Cruz, 2002), but it could also include many other things.

CHON+ with $O/N \leq 2$ in the January, April, October, and July samples represented 80%, 78%, 69%, and 61% of the total CHON+ compounds, respectively, which might be caused by stronger photochemical degradation in July and October (Table S1). Additionally, the average values of O/N were around 1.6, 1.8, 2.0, and 2.5, respectively, showing the same trend as that of CHON−. Apart from that, the most abundant CHON+ compounds in the July and October samples possessed higher O/N ratios and larger carbon numbers than those in the January and April samples, indicating different sources for these compounds. The 22%, 23%, 15%, and 17% of CHON+ compounds were monoaromatics, and 19%, 9%, 12%, and 13% were polycyclic aromatics for January, April, July, and October, respectively. Benzamide (C_7H_7NO), 4-Hydroxy-benzene acetonitrile (C_8H_7NO), and 3-(4-Hydroxyphenyl) propionitrile (C_9H_7NO), from biomass burning (Ma & Hays, 2008), were high in abundances during all four sampling periods.

3.4. CHOS and CHONS Compounds

Depending on the collection month, there were 307–413 CHOS− compounds and 169–300 CHONS− compounds, whose molecular weights centered around 120–440 Da and 160–450 Da, respectively (Figure 1). The CHONS− compounds showed higher masses than CHOS− because of the presence of one or two additional nitrate groups (Tao et al., 2014; Wang et al., 2016). The majority of the CHOS− and CHONS− compounds possessed higher H/C and O/C values ($0.3 < H/C < 3$ and $0 < O/C < 2$) than the CHO− compounds (Figures 5 and S5). Only about 18% of sulfur-containing compounds detected in ESI−, that is, CHOS− and CHONS−, belonged to monocyclic ($2.50 \leq Xc < 2.71$) or polycyclic ($2.71 \leq Xc$) aromatics with an average RDBE of 10, and the majority of them were in the triangle region of $0.3 < H/C < 1.6$ and $0 < O/C < 0.6$, indicating their low degrees of saturation and oxidation.

About 81–84% of CHOS− and 53–65% of CHONS− compounds possessed enough oxygen atoms to allow assignment of $-OSO_3H$ and/or $-ONO_2$ groups in their formulas, which can be regarded as OSs or nitrooxy-OSs (Lin et al., 2012; O'Brien et al., 2014; Wang et al., 2016). Comparing our results for $CHOS_1-$ compounds ($O/S \geq 4$) to an earlier study on SOA from biodiesel and diesel fuel (Blair et al., 2017), a sum of 213–254

Table 2
Number of (Nitrooxy-) OSs From Different Formation Pathways

	Number (percentage) of OSs from plausible reactant − product pairs			
Time	CHO ($+SO_4^{2-}$) → CHOS	CHON ($-NO_3^-$, $+HSO_4^-$) → CHOS	CHON ($+SO_4^{2-}$) → CHONS	CHONS ($+H_2O$, $-HNO_3$) → CHOS
April 2015	153 (53%)	66 (23%)	12 (10%)	99 (79%)
July 2014	139 (54%)	34 (13%)	3 (3%)	76 (80%)
October 2014	176 (57%)	72 (23%)	10 (7%)	108 (78%)
January 2015	176 (51%)	97 (28%)	17 (11%)	132 (83%)

identical formulas were found, accounting for 70–80% of the total number and 69–82% of the total abundance of the $CHOS_1-$ compounds observed here. Nonetheless, previous studies have shown that many of these species can also be formed from biogenic precursors, for example, $C_5H_{10}O_5S$ (derived from isoprene), $C_7H_{12}O_6S$ (derived from α-pinene), and $C_9H_{16}O_6S$ (derived from limonene or β-caryophyllene) (Chan et al., 2011; Riva et al., 2016; Surratt et al., 2008). The possibly mixed anthropogenic and biogenic origin of OSs leads to a great complexity and, thus, uncertainty in judging their sources. On the other hand, OSs of $C_5H_{12}O_7S$ (derived only from biogenic isoprene to the best of our knowledge) and nitrooxy-OSs of $C_{10}H_{17}NO_7S$ (derived only from biogenic α-pinene, β-pinene, α-terpinene, or terpinolene to the best of our knowledge) (Surratt et al., 2008) showed high abundances in each of the four-month samples, clearly indicating an influence of biogenic emissions on organic aerosol chemistry in Shanghai.

Lin et al. (2012) and O'Brien et al. (2014) concluded the importance of the epoxide formation pathway for OSs and nitrooxy-OSs by examining the presence of precursor-product pairs of the CHOS− (or CHONS−) and the corresponding CHO− (CHON−) compounds. The epoxide pathway necessitates that both OS and a corresponding compound with multiple hydroxyl groups are present, because nucleophilic attack to an epoxide from both sulfates and water molecules can occur in the aerosol phase. In this study, a similar analysis indicates that 51–57% of OSs existed with corresponding CHO− compounds with multiple hydroxyl groups (Table 2), similar to what was observed in Bakersfield (O'Brien et al., 2014) but slightly lower than those in the Pearl River Delta Region and Taiwan (Lin et al., 2012), suggesting that the epoxide formation pathway is an important formation route for the OSs observed in urban Shanghai. Recently, a direct formation of OSs from HOMs and/or peroxyradicals was suggested (Brüggemann et al., 2017). Because a number of HOMs were detected in all Shanghai samples, as discussed earlier, the direct formation mechanism may have also played a significant role in OS formation in addition to the epoxide formation pathway. In contrast to the CHOS−, only a small fraction of nitrooxy-OSs (3–11%) existed with the corresponding CHON− compounds with multiple hydroxyl groups, similar to those in the Pearl River Delta Region (3–15%) and Taiwan (0–6%) (Lin et al., 2012) but far lower than those in Bakersfield (27–42%) (O'Brien et al., 2014), implying that the epoxide pathway is insignificant for the formation of nitrooxy-OSs in Shanghai. In addition, organonitrates can be efficiently converted to OSs via hydrolysis of organonitrates with a sulfate group on ambient SOA (Hu, Darer, & Elrod, 2011), and 13–28% of OSs could be derived from this pathway in this study. It was also shown that organonitrates usually hydrolyze more rapidly than OSs (Hu et al., 2011). Hence, hydrolysis of nitrooxy-OSs could have also contributed to the abundance of OSs. In our study, on average 78–83% of the nitrooxy-OSs and their corresponding OSs were present (Table 2), highlighting the hydrolysis of the nitrooxy groups.

In ESI+, sulfur-containing compounds including CHOS+ and CHONS+ accounted for the lowest percentage, in terms of both number (Tables S2–S5) and abundance (Figure 2). Only 41–140 CHOS+ and 80–133 CHONS+ were detected in Shanghai samples. The majority of CHOS+ and CHONS+ compounds were characterized with low degrees of oxidation and saturation, and with an average RDBE of 8 and 5, respectively. In addition, more than 85% of the sulfur-containing compounds possessed $(S + N)/O \geq 0.5$, indicating that reduced nitrogen or sulfur functional groups were present in the chemical structure. CHOS+ and CHONS+ compounds (36–56%) had $Xc \geq 2.50$, indicating that they were aromatics containing reduced sulfur such as $C_{13}H_8OS$ ($Xc = 2.75$), $C_{14}H_{10}OS$ ($Xc = 2.75$), and $C_{16}H_{12}OS$ ($Xc = 2.78$), which were from fossil fuel combustion (Mead et al., 2015).

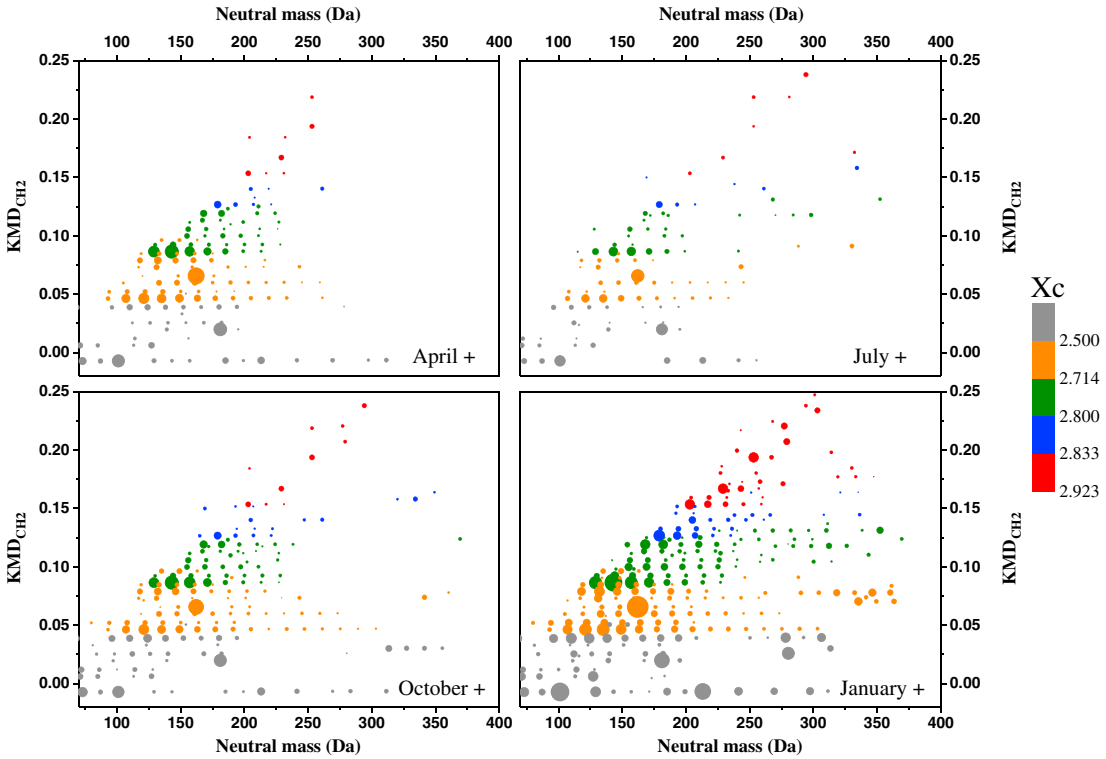

Figure 6. CH_2-Kendrick diagrams of CHN+. The color-coding indicates the Xc values calculated from equation (2). The grey, orange, green, blue, and red circles represent aliphatic compounds (Xc < 2.50), aromatics with a benzene core structure (2.50 ≤ Xc < 2.71), with a naphthalene (2.71 ≤ Xc < 2.80) core structure, with an anthracene (2.80 ≤ Xc < 2.83) core structure, and with a pyrene core structure (2.83 ≤ Xc < 2.92), respectively. The size of symbols is proportional to the fourth root of the abundance of a compound.

3.5. CHNS* (i.e., CHN, CHS, and CHNS) Compounds

Only 20–30 signals for CHNS*− compounds were detected in Shanghai, representing less than 0.4% of the total abundance of organic compounds (Figure 1). On the other hand, CHNS*+ accounted for around 20% of the total number (Tables S2–S5) and 22–44% of the total abundance (Figure 2), respectively.

Similarly, 115–304 CHN+ compounds were detected and many of them were likely amines, which are readily protonated (Rincón et al., 2012). Figure 6 shows the KMD diagrams for the CHN+ compounds, giving the most intense signals in the molecular weight range from 120 to 220 Da. In the KMD diagrams, molecules that differ only in the number of $-CH_2$ groups exhibit the same KMD_{CH2} values and appear on the same horizontal line, suggesting that these molecules have the same degree of unsaturation. In Figure 6, aliphatic compounds, such as triethylamine ($C_6H_{15}N$) and dodecanenitrile ($C_{12}H_{23}N$), appeared in the KMD_{CH2} range of −0.01–0.05; aromatic compounds with a benzene core structure, such as nicotine ($C_{10}H_{14}N_2$) and dimethyl toluidine ($C_9H_{13}N$), were observed in the KMD_{CH2} range of 0.05–0.10; and polycyclic aromatics with a naphthalene core structure, such as 1-naphthalenamine ($C_{10}H_9N$), including nitrogen-heterocyclic compounds such as quinoline (C_9H_7N), were found in the KMD_{CH2} range of 0.09–0.14. Apart from that, a few polycyclic aromatic compounds with an anthracene core structure (in the KMD_{CH2} range of 0.13–0.16) or with a pyrene core structure (in the KMD_{CH2} range of 0.15–0.25) were detected. These results suggest that the higher values of KMD_{CH2} correspond to the more complex aromatic compounds. Overall, the number of aliphatics accounted for 20–28% of the total CHN+ compounds, in contrast to 30–37% for monoaromatics and 36–49% for the polycyclic aromatics. The January samples contained the most aromatic CHN+ in terms of number and abundance, which were probably from biomass burning (Figure 1) (Ge et al., 2011; Schmeltz & Hoffmann, 1977; Simoneit et al., 2003).

Further VK diagrams for the CHN+ compounds are shown in Figure S6 where the N/C ratio is plotted versus the H/C ratio. These plots clearly separate the different classes of CHN+ according to the number of nitrogen

Table 3
Number of Nitrogen-Containing Compounds[a] Detected in ESI+ From Plausible Reactant-Product Pairs

	Number (percentage) of nitrogen-containing compounds from (both instances) plausible reactant − product pairs				
Time	R1	R2	R3	R4	Total unique formulas
April 2015	131 (22%)	116 (19%)	152 (25%)	209 (35%)	331 (55%)
July 2014	85 (15%)	84 (15%)	87 (15%)	118 (21%)	202 (35%)
October 2014	151 (16%)	123 (13%)	228 (24%)	276 (29%)	424 (45%)
January 2015	194 (17%)	142 (13%)	438 (39%)	466 (41%)	651 (57%)

[a]Compounds include CHON, CHONS, CHNS, and CHN.

atoms and the degree of unsaturation. Aromatic compounds, especially the polycyclic aromatic compounds, can be found at the lower left corner of the VK diagram, due to their low degree of saturation.

In areas where anthropogenic NH_3 emissions mix with anthropogenic or biogenic SOAs, reduced nitrogen can be added to organic molecules via imine formation reactions, replacing carbonyl oxygen atoms with NH groups (R1) (Nizkorodov et al., 2011; O'Brien et al., 2013). This pathway was verified previously in laboratory studies through heterogeneous uptake and reaction of gaseous ammonia with wet SOA particles (Laskin et al., 2010). The resulting imines can undergo additional cyclization reactions (R2) in the condensed aqueous phase SOAs through reactions with a second carbonyl group in the same compound. In addition, the resulting imines can also react with another carbonyl-containing compound forming substituted imines (R3). Then, the substituted imines from the R2 and R3 reactions can undergo additional disproportionation reactions (R4) (Laskin et al., 2010; Nizkorodov et al., 2011). Reactions R1–R4 are presented in Scheme S1 in the supporting information. The potential relevance of these reactions in forming nitrogen-containing compounds, including CHN+, CHON+, CHONS+, and CHNS+, was investigated according to the mass difference between the reactants and products in reactions R1–R4 and the prerequisite that only 178–254 compounds were found to contain at least one carbonyl functional group using pentafluorobenzylhydroxylamine derivatization. The number of precursor-product pairs for reactions R1–R4 is tabulated in Table 3, in which "total unique formulas" show the total number of unique nitrogen-containing compounds that can be explained by one of the reactions R1–R4, due to large overlaps. Approximately 35–57% of the nitrogen-containing compounds, accounting for 34–70% of the total abundance, could be explained by this type of chemistry. The results showed clear seasonal variations, the highest for the January samples and the lowest for the July samples in terms of both number and abundance, indicating that these reactions played more important roles in the formation of compounds containing reduced nitrogen groups in the January and April samples. It is likely that ammonia was involved in the chemical transformation of particulate organics in Shanghai, the same as in Bakersfield (O'Brien et al., 2013).

The number of CHS+ compounds ranged between 48 and 67, containing likely thiols, thioethers (R-S-R), thiophenols, or disulfides (R-S-S-R) (Rincón et al., 2012). Almost all tentatively identified CHS+ were reduced S-containing aromatics with $Xc \geq 2.50$, and the majority of them (82%–91%) belonged to polycyclic aromatics ($Xc \geq 2.71$). For example, $C_{12}H_8S$, which was the most abundant CHS+ compound in the January, April, and October samples and the second most abundant CHS+ compound in July samples, was likely dibenzothiophene from the vehicle emissions (Wingfors et al., 2001).

In addition, 29–47 CHNS+ formulas have been determined, possibly indicating the presence of sulfur-containing amines. CHNS+ compounds (48%, 26%, 15%, and 23%) were aromatics ($Xc \geq 2.50$) in the January, April, July, and October samples, respectively, also showing the same trend with other aromatics.

3.6. Pollution Case in October 2014

One pollution case was observed in October 2014, during which a significant contrast in air quality was observed between clean and polluted days (Table S1 and Figure 7a). Hence, this case is selected to elucidate the evolution of OAs. Figure 7a shows the average concentrations of O_3, SO_2, NO_2, and $PM_{2.5}$ in the same time interval as that for the October filter samples. On polluted days, SO_2, NO_2, and $PM_{2.5}$ were in high concentrations. Additionally, the particulate organics were richer in terms of both number (Figure 7b) and abundance

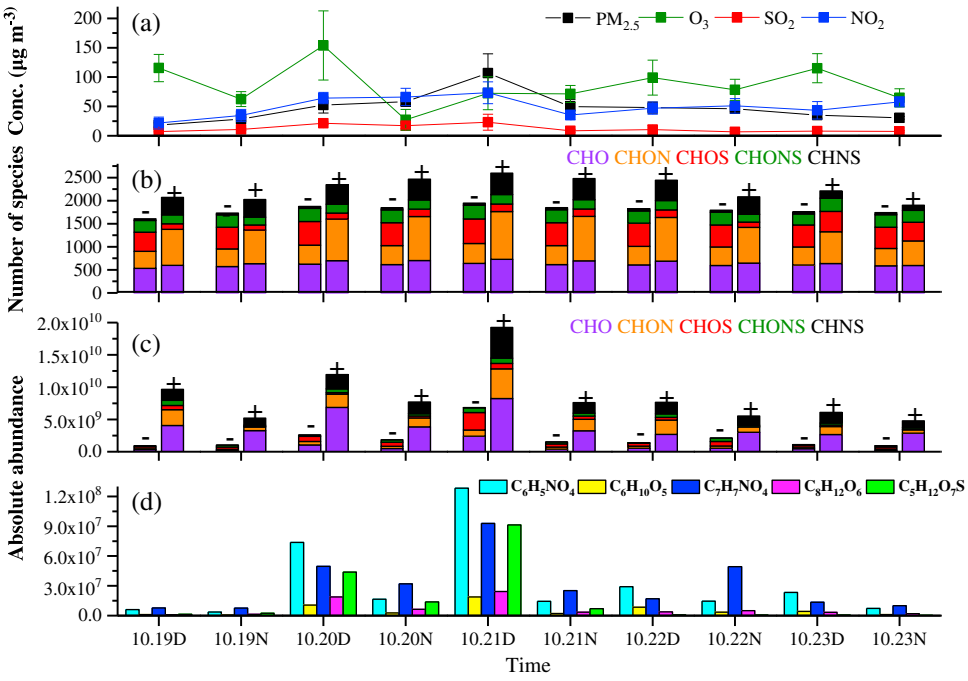

Figure 7. (a) The average concentrations of O_3, SO_2, NO_2, and $PM_{2.5}$ in the same time interval as that for the October filter samples. (b) Number of ESI− and ESI+ species in different categories. (c) Abundance of ESI− and ESI+ species in different categories. (d) Abundance of selected tentatively identified ESI− tracers in the October samples. The signs of minus (−) and plus (+) denote compounds detected in ESI− and ESI+, respectively.

(Figure 7c). The abundance of selected tentatively identified tracers was further examined in Figure 7d: $C_6H_{10}O_5$ likely correspond to anhydrosugars with several isomers including levoglucosan, mannosan, galactosan, and 1,6-anhydro-β-D-glucofuranose that are regarded as markers for biomass burning (Kourtchev et al., 2016; Pashynska et al., 2002); $C_6H_5NO_4$ is probably a mixture of isomers of nitrocatechols from mixed anthropogenic sources, for example, biomass and vehicular emissions; $C_7H_7NO_4$ is likely methyl-nitrocatechols usually selected as an important marker for biomass burning OAs, which is formed from *m*-cresol emitted during biomass burning as well as diesel exhaust (Iinuma et al., 2010; Lin et al., 2016); 3-methyl-1, 2, 3-butanetricarboxylic acid (3-MBTCA) can potentially explain the molecular formula $C_8H_{12}O_6$, an OH radical-initiated oxidation product of α- and β-pinene regarded as a tracer for biogenic SOA (Brüggemann et al., 2017; Kourtchev et al., 2013; Szmigielski et al., 2007); and $C_5H_{12}O_7S$ could be isoprene epoxydiol organosulfate ester (IEPOX-OS) formed through reactions between SOx (SO_2 + SO_4^{2-}) and isoprene oxidation products (Budisulistiorini et al., 2015; Pye et al., 2013; Surratt et al., 2008). The assignment of the exact identity for these molecular formulas was not based on MS/MS analysis or standard analysis; however, the suggested compounds (except for 3-MBTCA) have been previously identified in high concentrations in aerosol samples in Shanghai (Li et al., 2016; Ma et al., 2014), adding credence to our assignment. Compared with those in the daytime of 19 October, the abundances of anhydrosugars, nitrocatechols, methyl-nitrocatechols, 3-MBTCA, and IEPOX-OS increased by a factor of 19, 21, 12, 25, and 68, respectively, on the polluted day (21 October) with the highest $PM_{2.5}$ concentrations, indicating that both anthropogenic and biogenic emissions made contributions to the OAs in this pollution case.

4. Conclusions

The molecular composition of the organic fraction in atmospheric particles collected in July and October 2014 and January and April 2015 at an urban site in Shanghai was investigated using UHPLC coupled to HESI-Orbitrap MS. Compared with direct injection measurements by UHRMS in previous studies (Lin et al., 2012; Lin et al., 2012; O'Brien et al., 2013; O'Brien et al., 2014), the UHPLC separation used in our study reduced

potential ion suppression effects and, thus, allowed us to retrieve semiquantitative information on organic compounds in the collected particles. In total, 810–1,510 (ESI−) and 860–1,790 (ESI+) chemical formulas of organic compounds were assigned.

The chemical characteristics of OAs in urban Shanghai showed clear differences among different months and between daytime and nighttime. January samples contained the most organics in terms of both number and abundance. In contrast, the number and abundance of organic compounds in the July samples were by far the lowest. In addition, a significant number of monoaromatics and polycyclic aromatics were detected in each of the four months' samples. Again, the highest amount was observed for the January samples (42% of the total number in ESI− and 49% of the total number in ESI+) and the lowest for the July samples (32% of the total number in ESI− and 35% of the total number in ESI+), suggesting that biomass burning and fossil fuel combustion made important contributions to the OAs in urban Shanghai. In general, the number of CHO− and CHOS− compounds was higher for the daytime samples, whereas CHONS− compounds were predominant in the nighttime samples. This contrasting temporal behavior might indicate different formation pathways of these compound classes, for example, daytime photochemistry versus nitrate radical nighttime chemistry.

We hypothesize that a large range of CHO species in Shanghai were associated with BBOA directly emitted into the atmosphere. Subsequent processing by multistep oxidation reactions might have then resulted in the production of SV-OOA and LV-OOA compounds. In our study, a significant number of HOMs were determined. These compounds may have been derived from oxidation reactions between OH radicals and aromatics such as benzene, toluene, xylenes, and trimethylbenzenes. The presence of these HOMs in Shanghai samples suggests that photooxidation of AVOCs might be an important source for highly oxygenated compounds in urban environments.

The CHOS and CHONS compounds were mainly detected in the ESI−; thus, most of them were attributed to OSs and nitrooxy-OSs. Since a significant number of OSs could derive from both anthropogenic and biogenic precursors, it is premature to judge their exact sources at this point. Nonetheless, a precursor-product pair analysis pointed toward the conclusion that the epoxide intermediate pathway dominated for the formation of OSs. A similar precursor-product pair analyses suggested that 35–57% of the nitrogen-containing compounds (accounting for 34–70% of the total abundances) detected in ESI+ might have been formed through ammonia-carbonyl chemistry, followed by cyclization and disproportionation reactions. Compared to a previous study in Bakersfield, CA, USA, far more reduced nitrogen-containing compounds were detected (O'Brien et al., 2013; O'Brien et al., 2014), highlighting one of the major characteristics of urban aerosols in Shanghai.

In summary, anthropogenic emissions were shown to have a larger impact on organic aerosol composition in urban Shanghai compared with biogenic primary and secondary sources. Nonetheless, regional transport could have been at least partly responsible for the observed seasonal variations in chemical characteristics of OAs, because many of the most abundant organics observed in our study (Table 1) are likely formed from biomass burning processes, which are normally fairly negligible in the Shanghai area (Li et al., 2016).

Acknowledgments
This study was financially supported by the National Natural Science Foundation of China (21222703, 21561130150, 41575113, and 91644213), the Ministry of Science and Technology of China (2012YQ220113-4), and the Cyrus Tang Foundation (CTF-FD2014001). L.Wang thanks the Royal Society Newton Advanced Fellowship (NA140106). C. George thanks the support by the European Research Council under the European Union's Seventh Framework Programme (FP/2007-2013)/ERC grant agreement 290852-AIRSEA, the Marie Curie International Research Staff Exchange project AMIS (grant 295132), and the Region Auvergne-Rhône-Alpes. All data are made available as part of the supporting information.

References

Altieri, K. E., Hastings, M. G., Peters, A. J., & Sigman, D. M. (2012). Molecular characterization of water soluble organic nitrogen in marine rainwater by ultra-high resolution electrospray ionization mass spectrometry. *Atmospheric Chemistry and Physics*, *12*(7), 3557–3571. https://doi.org/10.5194/acp-12-3557-2012

Bateman, A. P., Nizkorodov, S. A., Laskin, J., & Laskin, A. (2009). Time-resolved molecular characterization of limonene/ozone aerosol using high-resolution electrospray ionization mass spectrometry. *Physical Chemistry Chemical Physics*, *11*(36), 7931–7942. https://doi.org/10.1039/b905288g

Bianchi, F., Tröstl, J., Junninen, H., Frege, C., Henne, S., Hoyle, C. R., … Baltensperger, U. (2016). New particle formation in the free troposphere: A question of chemistry and timing. *Science*, *352*(6289), 1109–1112. https://doi.org/10.1126/science.aad5456

Blair, S. L., MacMillan, A. C., Drozd, G. T., Goldstein, A. H., Chu, R. K., Paša-Tolić, L., … Nizkorodov, S. A. (2017). Molecular characterization of organosulfur compounds in biodiesel and diesel fuel secondary organic aerosol. *Environmental Science & Technology*, *51*(1), 119–127. https://doi.org/10.1021/acs.est.6b03304

Borrás, E., & Tortajada-Genaro, L. A. (2012). Determination of oxygenated compounds in secondary organic aerosol from isoprene and toluene smog chamber experiments. *International Journal of Environmental Analytical Chemistry*, *92*(1), 110–124. https://doi.org/10.1080/03067319.2011.572164

Brüggemann, M., Poulain, L., Held, A., Stelzer, T., Zuth, C., Richters, S., … Hoffmann, T. (2017). Real-time detection of highly oxidized organosulfates and BSOA marker compounds during the F-BEACh 2014 field study. *Atmospheric Chemistry and Physics*, *17*(2), 1453–1469. https://doi.org/10.5194/acp-17-1453-2017

Budisulistiorini, S. H., Li, X., Bairai, S. T., Renfro, J., Liu, Y., Liu, Y. J., … Surratt, J. D. (2015). Examining the effects of anthropogenic emissions on isoprene-derived secondary organic aerosol formation during the 2013 southern oxidant and aerosol study (SOAS) at the Look Rock, Tennessee ground site. *Atmospheric Chemistry and Physics*, *15*(15), 8871–8888. https://doi.org/10.5194/acp-15-8871-2015

Cech, N. B., & Enke, C. G. (2001). Practical implications of some recent studies in electrospray ionization fundamentals. *Mass Spectrometry Reviews*, *20*(6), 362–387. https://doi.org/10.1002/mas.10008

Chan, M. N., Surratt, J. D., Chan, A. W. H., Schilling, K., Offenberg, J. H., Lewandowski, M., … Seinfeld, J. H. (2011). Influence of aerosol acidity on the chemical composition of secondary organic aerosol from β-caryophyllene. *Atmospheric Chemistry and Physics*, *11*(4), 1735–1751. https://doi.org/10.5194/acp-11-1735-2011

Cheng, Y., Li, S.-M., & Leithead, A. (2006). Chemical characteristics and origins of nitrogen-containing organic compounds in $PM_{2.5}$ aerosols in the lower Fraser Valley. *Environmental Science & Technology*, *40*(19), 5846–5852. https://doi.org/10.1021/es0603857

Fuller, S. J., Zhao, Y., Cliff, S. S., Wexler, A. S., & Kalberer, M. (2012). Direct surface analysis of time-resolved aerosol impactor samples with ultrahigh-resolution mass spectrometry. *Analytical Chemistry*, *84*(22), 9858–9864. https://doi.org/10.1021/ac3020615

Ge, X., Wexler, A. S., & Clegg, S. L. (2011). Atmospheric amines—Part I. A review. *Atmospheric Environment*, *45*(3), 524–546. https://doi.org/10.1016/j.atmosenv.2010.10.012

Goldstein, A. H., & Galbally, I. E. (2007). Known and unexplored organic constituents in the Earth's atmosphere. *Environmental Science & Technology*, *41*(5), 1514–1521. https://doi.org/10.1021/es072476p

Gómez-González, Y., Wang, W., Vermeylen, R., Chi, X., Neirynck, J., Janssens, I. A., … Claeys, M. (2012). Chemical characterisation of atmospheric aerosols during a 2007 summer field campaign at Brasschaat, Belgium: Sources and source processes of biogenic secondary organic aerosol. *Atmospheric Chemistry and Physics*, *12*(1), 125–138. https://doi.org/10.5194/acp-12-125-2012

Hatch, L. E., Creamean, J. M., Ault, A. P., Surratt, J. D., Chan, M. N., Seinfeld, J. H., … Prather, K. A. (2011). Measurements of isoprene-derived organosulfates in ambient aerosols by aerosol time-of-flight mass spectrometry—Part 1: Single particle atmospheric observations in Atlanta. *Environmental Science & Technology*, *45*(12), 5105–5111. https://doi.org/10.1021/es103944a

Hu, K. S., Darer, A. I., & Elrod, M. J. (2011). Thermodynamics and kinetics of the hydrolysis of atmospherically relevant organonitrates and organosulfates. *Atmospheric Chemistry and Physics*, *11*(16), 8307–8320. https://doi.org/10.5194/acp-11-8307-2011

Hu, M., Krauss, M., Brack, W., & Schulze, T. (2016). Optimization of LC-Orbitrap-HRMS acquisition and MZmine 2 data processing for nontarget screening of environmental samples using design of experiments. *Analytical and Bioanalytical Chemistry*, *408*(28), 7905–7915. https://doi.org/10.1007/s00216-016-9919-8

Huang, C., Chen, C. H., Li, L., Cheng, Z., Wang, H. L., Huang, H. Y., … Chen, Y. R. (2011). Emission inventory of anthropogenic air pollutants and VOC species in the Yangtze River Delta region, China. *Atmospheric Chemistry and Physics*, *11*(9), 4105–4120. https://doi.org/10.5194/acp-11-4105-2011

Huang, R. J., Zhang, Y., Bozzetti, C., Ho, K. F., Cao, J. J., Han, Y., … Prévôt, A. S. (2014). High secondary aerosol contribution to particulate pollution during haze events in China. *Nature*, *514*(7521), 218–222. https://doi.org/10.1038/nature13774

Hughey, C. A., Hendrickson, C. L., Rodgers, R. P., Marshall, A. G., & Qian, K. N. (2001). Kendrick mass defect spectrum: A compact visual analysis for ultrahigh-resolution broadband mass spectra. *Analytical Chemistry*, *73*(19), 4676–4681. https://doi.org/10.1021/ac010560w

Iinuma, Y., Boge, O., Grafe, R., & Herrmann, H. (2010). Methyl-nitrocatechols: Atmospheric tracer compounds for biomass burning secondary organic aerosols. *Environmental Science & Technology*, *44*(22), 8453–8459. https://doi.org/10.1021/es102938a

Jakober, C. A., Charles, M. J., Kleeman, M. J., & Green, P. G. (2006). LC-MS analysis of carbonyl compounds and their occurrence in diesel emissions. *Analytical Chemistry*, *78*(14), 5086–5093. https://doi.org/10.1021/ac060301c

Jimenez, J. L., Canagaratna, M. R., Donahue, N. M., Prevot, A. S. H., Zhang, Q., Kroll, J. H., … Worsnop, D. R. (2009). Evolution of organic aerosols in the atmosphere. *Science*, *326*(5959), 1525–1529. https://doi.org/10.1126/science.1180353

Katajamaa, M., Miettinen, J., & Oresic, M. (2006). MZmine: Toolbox for processing and visualization of mass spectrometry based molecular profile data. *Bioinformatics*, *22*(5), 634–636. https://doi.org/10.1093/bioinformatics/btk039

Kendrick, E. (1963). A mass scale based on CH_2 = 14.0000 for high resolution mass apectrometry of organic compounds. *Analytical Chemistry*, *35*(13), 2146–2154. https://doi.org/10.1021/ac60206a048

Kim, S., Kramer, R. W., & Hatcher, P. G. (2003). Graphical method for analysis of ultrahigh-resolution broadband mass spectra of natural organic matter, the van Krevelen diagram. *Analytical Chemistry*, *75*(20), 5336–5344. https://doi.org/10.1021/ac034415p

Kind, T., & Fiehn, O. (2007). Seven golden rules for heuristic filtering of molecular formulas obtained by accurate mass spectrometry. *BMC Bioinformatics*, *8*(1), 105. https://doi.org/10.1186/1471-2105-8-105

Kitanovski, Z., Grgic, I., Vermeylen, R., Claeys, M., & Maenhaut, W. (2012). Liquid chromatography tandem mass spectrometry method for characterization of monoaromatic nitro-compounds in atmospheric particulate matter. *Journal of Chromatography. A*, *1268*, 35–43. https://doi.org/10.1016/j.chroma.2012.10.021

Kitanovski, Z., Grgic, I., Yasmeen, F., Claeys, M., & Cusak, A. (2012). Development of a liquid chromatographic method based on ultraviolet-visible and electrospray ionization mass spectrometric detection for the identification of nitrocatechols and related tracers in biomass burning atmospheric organic aerosol. *Rapid Communications in Mass Spectrometry*, *26*(7), 793–804. https://doi.org/10.1002/rcm.6170

Kourtchev, I., Doussin, J. F., Giorio, C., Mahon, B., Wilson, E. M., Maurin, N., … Kalberer, M. (2015). Molecular composition of fresh and aged secondary organic aerosol from a mixture of biogenic volatile compounds: A high-resolution mass spectrometry study. *Atmospheric Chemistry and Physics*, *15*(10), 5683–5695. https://doi.org/10.5194/acp-15-5683-2015

Kourtchev, I., Fuller, S., Aalto, J., Ruuskanen, T. M., McLeod, M. W., Maenhaut, W., … Kalberer, M. (2013). Molecular composition of boreal forest aerosol from Hyytiala, Finland, using ultrahigh resolution mass spectrometry. *Environmental Science & Technology*, *47*(9), 4069–4079. https://doi.org/10.1021/es3051636

Kourtchev, I., Godoi, R. H. M., Connors, S., Levine, J. G., Archibald, A. T., Godoi, A. F. L., … Kalberer, M. (2016). Molecular composition of organic aerosols in central Amazonia: An ultra-high-resolution mass spectrometry study. *Atmospheric Chemistry and Physics*, *16*(18), 11,899–11,913 . https://doi.org/10.5194/acp-16-11899-2016

Kroll, J. H., Donahue, N. M., Jimenez, J. L., Kessler, S. H., Canagaratna, M. R., Wilson, K. R., … Worsnop, D. R. (2011). Carbon oxidation state as a metric for describing the chemistry of atmospheric organic aerosol. *Nature Chemistry*, *3*(2), 133–139. https://doi.org/10.1038/nchem.948

Kroll, J. H., & Seinfeld, J. H. (2008). Chemistry of secondary organic aerosol: Formation and evolution of low-volatility organics in the atmosphere. *Atmospheric Environment*, *42*(16), 3593–3624. https://doi.org/10.1016/j.atmosenv.2008.01.003

Laskin, A., Laskin, J., & Nizkorodov, S. A. (2015). Chemistry of atmospheric brown carbon. *Chemical Reviews*, *115*(10), 4335–4382. https://doi.org/10.1021/cr5006167

Laskin, A., Smith, J. S., & Laskin, J. (2009). Molecular characterization of nitrogen-containing organic compounds in biomass burning aerosols using high-resolution mass spectrometry. *Environmental Science & Technology*, *43*(10), 3764–3771. https://doi.org/10.1021/es803456n

Laskin, J., Laskin, A., Roach, P. J., Slysz, G. W., Anderson, G. A., Nizkorodov, S. A., … Nguyen, L. Q. (2010). High-resolution desorption electrospray ionization mass spectrometry for chemical characterization of organic aerosols. *Analytical Chemistry*, *82*(5), 2048–2058. https://doi.org/10.1021/ac902801f

Li, X., Jiang, L., Hoa, L. P., Lyu, Y., Xu, T., Yang, X., … Herrmann, H. (2016). Size distribution of particle-phase sugar and nitrophenol tracers during severe urban haze episodes in Shanghai. *Atmospheric Environment*, *145*, 115–127. https://doi.org/10.1016/j.atmosenv.2016.09.030

Lin, P., Aiona, P. K., Li, Y., Shiraiwa, M., Laskin, J., Nizkorodov, S. A., & Laskin, A. (2016). Molecular characterization of brown carbon in biomass burning aerosol particles. *Environmental Science & Technology*, *50*(21), 11,815–11,824. https://doi.org/10.1021/acs.est.6b03024

Lin, P., Rincon, A. G., Kalberer, M., & Yu, J. Z. (2012). Elemental composition of HULIS in the Pearl River Delta Region, China: Results inferred from positive and negative electrospray high resolution mass spectrometric data. *Environmental Science & Technology*, *46*(14), 7454–7462. https://doi.org/10.1021/es300285d

Lin, P., Yu, J. Z., Engling, G., & Kalberer, M. (2012). Organosulfates in humic-like substance fraction isolated from aerosols at seven locations in East Asia: A study by ultra-high-resolution mass spectrometry. *Environmental Science & Technology*, *46*(24), 13,118–13,127. https://doi.org/10.1021/es303570v

Ma, Y., & Hays, M. D. (2008). Thermal extraction-two-dimensional gas chromatography-mass spectrometry with heart-cutting for nitrogen heterocyclics in biomass burning aerosols. *Journal of Chromatography. A*, *1200*(2), 228–234. https://doi.org/10.1016/j.chroma.2008.05.078

Ma, Y., Xu, X. K., Song, W. H., Geng, F. H., & Wang, L. (2014). Seasonal and diurnal variations of particulate organosulfates in urban Shanghai, China. *Atmospheric Environment*, *85*, 152–160. https://doi.org/10.1016/j.atmosenv.2013.12.017

Mead, R. N., Felix, J. D., Avery, G. B., Kieber, R. J., Willey, J. D., & Podgorski, D. C. (2015). Characterization of CHOS compounds in rainwater from continental and coastal storms by ultrahigh resolution mass spectrometry. *Atmospheric Environment*, *105*, 162–168. https://doi.org/10.1016/j.atmosenv.2015.01.057

Mohr, C., Lopez-Hilfiker, F. D., Zotter, P., Prévôt, A. S., Xu, L., Ng, N. L., … Thornton, J. A. (2013). Contribution of nitrated phenols to wood burning brown carbon light absorption in Detling, United Kingdom during winter time. *Environmental Science & Technology*, *47*(12), 6316–6324. https://doi.org/10.1021/es400683v

Molteni, U., Bianchi, F., Klein, F., El Haddad, I., Frege, C., Rossi, M. J., … Baltensperger, U. (2016). Formation of highly oxygenated organic molecules from aromatic compounds. *Atmospheric Chemistry and Physics Discussions*, 1–39. https://doi.org/10.5194/acp-2016-1126

Nguyen, T. B., Bateman, A. P., Bones, D. L., Nizkorodov, S. A., Laskin, J., & Laskin, A. (2010). High-resolution mass spectrometry analysis of secondary organic aerosol generated by ozonolysis of isoprene. *Atmospheric Environment*, *44*(8), 1032–1042. https://doi.org/10.1016/j.atmosenv.2009.12.019

Nguyen, T. B., Laskin, J., Laskin, A., & Nizkorodov, S. A. (2011). Nitrogen-containing organic compounds and oligomers in secondary organic aerosol formed by photooxidation of isoprene. *Environmental Science & Technology*, *45*(16), 6908–6918. https://doi.org/10.1021/es201611n

Nizkorodov, S. A., Laskin, J., & Laskin, A. (2011). Molecular chemistry of organic aerosols through the application of high resolution mass spectrometry. *Physical Chemistry Chemical Physics*, *13*(9), 3612–3629. https://doi.org/10.1039/c0cp02032j

Nozière, B., Ekström, S., Alsberg, T., & Holmström, S. (2010). Radical-initiated formation of organosulfates and surfactants in atmospheric aerosols. *Geophysical Research Letters*, *37*(5), L0580. https://doi.org/10.1029/2009GL041683

O'Brien, R. E., Laskin, A., Laskin, J., Liu, S., Weber, R., Russell, L. M., & Goldstein, A. H. (2013). Molecular characterization of organic aerosol using nanospray desorption/electrospray ionization mass spectrometry: CalNex 2010 field study. *Atmospheric Environment*, *68*, 265–272. https://doi.org/10.1016/j.atmosenv.2012.11.056

O'Brien, R. E., Laskin, A., Laskin, J., Rubitschun, C. L., Surratt, J. D., & Goldstein, A. H. (2014). Molecular characterization of S- and N-containing organic constituents in ambient aerosols by negative ion mode high-resolution nanospray desorption electrospray ionization mass spectrometry: CalNex 2010 field study. *Journal of Geophysical Research – Atmospheres*, *119*(22), 12,706–12,720. https://doi.org/10.1002/2014JD021955

Pashynska, V., Vermeylen, R., Vas, G., Maenhaut, W., & Claeys, M. (2002). Development of a gas chromatographic/ion trap mass spectrometric method for the determination of levoglucosan and saccharidic compounds in atmospheric aerosols. Application to urban aerosols. *Journal of Mass Spectrometry*, *37*(12), 1249–1257. https://doi.org/10.1002/jms.391

Pluskal, T., Castillo, S., Villar-Briones, A., & Oresic, M. (2010). MZmine 2: Modular framework for processing, visualizing, and analyzing mass spectrometry-based molecular profile data. *BMC Bioinformatics*, *11*(1), 395. https://doi.org/10.1186/1471-2105-11-395

Pöschl, U. (2005). Atmospheric aerosols: Composition, transformation, climate and health effects. *Angewandte Chemie, International Edition*, *44*(46), 7520–7540. https://doi.org/10.1002/anie.200501122

Pye, H. O., Pinder, R. W., Piletic, I. R., Xie, Y., Capps, S. L., Lin, Y. H., … Edney, E. O. (2013). Epoxide pathways improve model predictions of isoprene markers and reveal key role of acidity in aerosol formation. *Environmental Science & Technology*, *47*(19), 11,056–11,064. https://doi.org/10.1021/es402106h

Reinhardt, A., Emmenegger, C., Gerrits, B., Panse, C., Dommen, J., Baltensperger, U., … Kalberer, M. (2007). Ultrahigh mass resolution and accurate mass measurements as a tool to characterize oligomers in secondary organic aerosols. *Analytical Chemistry*, *79*(11), 4074–4082. https://doi.org/10.1021/ac062425v

Rincón, A. G., Calvo, A. I., Dietzel, M., & Kalberer, M. (2012). Seasonal differences of urban organic aerosol composition—An ultra-high resolution mass spectrometry study. *Environment and Chemistry*, *9*(3), 298–319. https://doi.org/10.1071/EN12016

Rissanen, M. P., Kurtén, T., Sipilä, M., Thornton, J. A., Kangasluoma, J., Sarnela, N., … Ehn, M. (2014). The formation of highly oxidized multifunctional products in the ozonolysis of cyclohexene. *Journal of the American Chemical Society*, *136*(44), 15596–15606. https://doi.org/10.1021/ja507146s

Riva, M., Budisulistiorini, S. H., Zhang, Z., Gold, A., & Surratt, J. D. (2016). Chemical characterization of secondary organic aerosol constituents from isoprene ozonolysis in the presence of acidic aerosol. *Atmospheric Environment*, *130*, 5–13. https://doi.org/10.1016/j.atmosenv.2015.06.027

Riva, M., Robinson, E. S., Perraudin, E., Donahue, N. M., & Villenave, E. (2015). Photochemical aging of secondary organic aerosols generated from the photooxidation of polycyclic aromatic hydrocarbons in the gas-phase. *Environmental Science & Technology*, *49*(9), 5407–5416. https://doi.org/10.1021/acs.est.5b00442

Roach, P. J., Laskin, J., & Laskin, A. (2010). Molecular characterization of organic aerosols using nanospray-desorption/electrospray ionization-mass spectrometry. *Analytical Chemistry*, *82*(19), 7979–7986. https://doi.org/10.1021/ac101449p

Romonosky, D. E., Li, Y., Shiraiwa, M., Laskin, A., Laskin, J., & Nizkorodov, S. A. (2017). Aqueous photochemistry of secondary organic aerosol of alpha-pinene and alpha-humulene oxidized with ozone, hydroxyl radical, and nitrate radical. *The Journal of Physical Chemistry. A*, *121*(6), 1298–1309. https://doi.org/10.1021/acs.jpca.6b10900

Rudich, Y., Donahue, N. M., & Mentel, T. F. (2007). Aging of organic aerosol: Bridging the gap between laboratory and field studies. *Annual Review of Physical Chemistry*, *58*(1), 321–352. https://doi.org/10.1146/annurev.physchem.58.032806.104432

Schindelka, J., Iinuma, Y., Hoffmann, D., & Herrmann, H. (2013). Sulfate radical-initiated formation of isoprene-derived organosulfates in atmospheric aerosols. *Faraday Discussions*, *165*, 237–259. https://doi.org/10.1039/c3fd00042g

Schmeltz, I., & Hoffmann, D. (1977). Nitrogen-containing compounds in tobacco and tobacco smoke. *Chemical Reviews*, *77*(3), 295–311. https://doi.org/10.1021/cr60307a001

Seinfeld, J. H., & Pankow, J. F. (2003). Organic atmospheric particulate material. *Annual Review of Physical Chemistry*, *54*(1), 121–140. https://doi.org/10.1146/annurev.physchem.54.011002.103756

Simoneit, B. R. T., Rushdi, A. I., bin Abas, M. R., & Didyk, B. M. (2003). Alkyl amides and nitriles as novel tracers for biomass burning. *Environmental Science & Technology*, *37*(1), 16–21, https://doi.org/10.1021/es020811y

Surratt, J. D., Gomez-Gonzalez, Y., Chan, A., Vermeylen, R., Shahgholi, M., Kleindienst, T., … Seinfeld, J. H. (2008). Organosulfate formation in biogenic secondary organic aerosol. *The Journal of Physical Chemistry. A*, *112*(36), 8345–8378. https://doi.org/10.1021/jp802310p

Szmigielski, R., Surratt, J. D., Gómez-González, Y., van der Veken, P., Kourtchev, I., Vermeylen, R., … Claeys, M. (2007). 3-methyl-1,2,3-butanetricarboxylic acid: An atmospheric tracer for terpene secondary organic aerosol. *Geophysical Research Letters*, *34*(24), L24811. https://doi.org/10.1029/2007GL031338

Tao, S., Lu, X., Levac, N., Bateman, A. P., Nguyen, T. B., Bones, D. L., … Yang, X. (2014). Molecular characterization of organosulfates in organic aerosols from shanghai and Los Angeles urban areas by nanospray-desorption electrospray ionization high-resolution mass spectrometry. *Environmental Science & Technology*, *48*(18), 10,993–11,001. https://doi.org/10.1021/es5024674

Tong, H., Kourtchev, I., Pant, P., Keyte, I. J., O'Connor, I. P., Wenger, J. C., … Kalberer, M. (2016). Molecular composition of organic aerosols at urban background and road tunnel sites using ultra-high resolution mass spectrometry. *Faraday Discussions*, *189*, 51–68. https://doi.org/10.1039/C5FD00206K

Tu, P., Hall, W. A., & Johnston, M. V. (2016). Characterization of highly oxidized molecules in fresh and aged biogenic secondary organic aerosol. *Analytical Chemistry*, *88*(8), 4495–4501. https://doi.org/10.1021/acs.analchem.6b00378

Vogel, A. L., Schneider, J., Muller-Tautges, C., Klimach, T., & Hoffmann, T. (2016). Aerosol chemistry resolved by mass spectrometry: Insights into particle growth after ambient new particle formation. *Environmental Science & Technology*, *50*(20), 10,814–10,822. https://doi.org/10.1021/acs.est.6b01673

Vogel, A. L., Schneider, J., Müller-Tautges, C., Phillips, G. J., Pöhlker, M. L., Rose, D., … Hoffmann, T. (2016). Aerosol chemistry resolved by mass spectrometry: Linking field measurements of cloud condensation nuclei activity to organic aerosol composition. *Environmental Science & Technology*, *50*(20), 10,823–10,832. https://doi.org/10.1021/acs.est.6b01675

Walser, M. L., Desyaterik, Y., Laskin, J., Laskin, A., & Nizkorodov, S. A. (2008). High-resolution mass spectrometric analysis of secondary organic aerosol produced by ozonation of limonene. *Physical Chemistry Chemical Physics*, *10*(7), 1009–1022. https://doi.org/10.1039/B712620D

Wang, L., Du, H. H., Chen, J. M., Zhang, M., Huang, X. Y., Tan, H. B., … Geng, F. H. (2013). Consecutive transport of anthropogenic air masses and dust storm plume: Two case events at Shanghai, China. *Atmospheric Research*, *127*, 22–33. https://doi.org/10.1016/j.atmosres.2013.02.011

Wang, X. K., Rossignol, S., Ma, Y., Yao, L., Wang, M. Y., Chen, J. M., … Wang, L. (2016). Molecular characterization of atmospheric particulate organosulfates in three megacities at the middle and lower reaches of the Yangtze River. *Atmospheric Chemistry and Physics*, *16*(4), 2285–2298. https://doi.org/10.5194/acp-16-2285-2016

Williams, P. I., Allan, J. D., Lobo, P., Coe, H., Christie, S., Wilson, C., … Rye, L. (2012). Impact of alternative fuels on emissions characteristics of a gas turbine engine - part 2: Volatile and semivolatile particulate matter emissions. *Environmental Science & Technology*, *46*(19), 10812–10819. https://doi.org/10.1021/es301899s

Wingfors, H., Sjodin, A., Haglund, P., & Brorstrom-Lunden, E. (2001). Characterisation and determination of profiles of polycyclic aromatic hydrocarbons in a traffic tunnel in Gothenburg, Sweden. *Atmospheric Environment*, *35*(36), 6361–6369. https://doi.org/10.1016/S1352-2310(01)00389-2

Wu, Z. G., Rodgers, R. P., & Marshall, A. G. (2004). Two- and three-dimensional van Krevelen diagrams: A graphical analysis complementary to the Kendrick mass plot for sorting elemental compositions of complex organic mixtures based on ultrahigh-resolution broadband Fourier transform ion cyclotron resonance mass measurements. *Analytical Chemistry*, *76*(9), 2511–2516. https://doi.org/10.1021/ac0355449

Xiao, S., Wang, M. Y., Yao, L., Kulmala, M., Zhou, B., Yang, X., … Wang, L. (2015). Strong atmospheric new particle formation in winter in urban Shanghai, China. *Atmospheric Chemistry and Physics*, *15*(4), 1769–1781. https://doi.org/10.5194/acp-15-1769-2015

Xu, W., & Zhang, R. (2012). Theoretical investigation of interaction of dicarboxylic acids with common aerosol nucleation precursors. *The Journal of Physical Chemistry. A*, *116*(18), 4539–4550. https://doi.org/10.1021/jp301964u

Yao, L., Wang, M.-Y., Wang, X.-K., Liu, Y.-J., Chen, H.-F., Zheng, J., … Wang, L. (2016). Detection of atmospheric gaseous amines and amides by a high-resolution time-of-flight chemical ionization mass spectrometer with protonated ethanol reagent ions. *Atmospheric Chemistry and Physics*, *16*(22), 14,527–14,543. https://doi.org/10.5194/acp-16-14527-2016

Yassine, M. M., Harir, M., Dabek-Zlotorzynska, E., & Schmitt-Kopplin, P. (2014). Structural characterization of organic aerosol using Fourier transform ion cyclotron resonance mass spectrometry: Aromaticity equivalent approach. *Rapid Communications in Mass Spectrometry*, *28*(22), 2445–2454. https://doi.org/10.1002/rcm.7038

Zha, S. P., Cheng, T. T., Tao, J., Zhang, R. J., Chen, J. M., Zhang, Y. W., … Du, J. F. (2014). Characteristics and relevant remote sources of black carbon aerosol in Shanghai. *Atmospheric Research*, *135*, 159–171.

Zhang, Q., Anastasio, C., & Jimemez-Cruz, M. (2002). Water-soluble organic nitrogen in atmospheric fine particles (PM2.5) from northern California. *Journal of Geophysical Research*, *107*(D11), 4112. https://doi.org/10.1029/2001JD000870